

Improvement adhesion and dispersion of microfibrillated lignocellulose compared to pure cellulose in poly(lactic-acid)

Master´s Thesis

For obtaining the academic degree
Dipl. Ing.

University of Natural resources and Life Sciences,
Vienna



Department for Material Science and Process
Engineering
Institute of Wood Technology and Renewable Resources
Tulln



Presented by

Ing. Winter Armin, BSc.

Keywords:

Lignocellulose, Cellulose, Poly(lactic-acid) (PLA), dispersion, adhesion, extrusion, polymer, composite

Abstract:

Growing ecological consciousness calls for efforts to develop new innovative and bio-based materials. Polymers synthesized from natural resource, enhanced with cellulose fibres had become more and more interesting. This class of materials is known as composites. Cellulose fibres have a different surface energy comparing to polymers. This prevents a good adhesion between fibre and polymer. Another disadvantage of cellulose is the agglomeration during processing mainly caused by hydrogen bonds. These clusters lead to an unfavourable distribution of the fibres in the material and thus prevent the optimal reinforcement ability. In order to improve miscibility as well as adhesion of the cellulose fibres, beech wood chips were produced in an organosolv process to produce lignocellulose. Through this process, lignin residues remain on the fibre. The unpolar lignin act as miscibility and adhesion promoter for the fibres and alters the mechanical properties of the Poly(lactic-acid) polymer.

Note of thanks

First of all, I want to thank my beloved wife Tanja. Thank you for standing by my side and your support. Your faith gave me strength and self-confidence to choose this path and I am very glad that you joined me on the way.

Next I want to thank my Supervisor Univ. Prof. Dipl.-Ing. Dr.nat.techn. Wolfgang Gindl-Altmatter, who gave me the Opportunity to work in his group. He revealed to me the world of bio-based materials and opened a new point of view, to look at the ingenuity of nature's workshop.

Special thanks go to my colleagues at the Institute of renewable resources and wood technology. To all the people working at the Institute for their help, starting from organizational issues to laboratory problems and for the hints, which helped me a lot to finish my task.

Especially I want to thank Dr. Dipl. -Ing. Stefan Veigel for his sharp mind and his readiness to share it with me.

Thanks also to Sabine Herzele, MSc. for her pre study on a similar subject and her enduring kindness and expertise on all the different topics of my work.

Also I want to thank Hannes Frech, Msc. from the Institute of natural engineering, no one is better suited to handle the deep mysteries of the extrusion process.

Thank you to the people on this institute who helped with different measurements issue concerning polymers.

Last but not least I want to thank my family and friends who shared their time with me. It is good to have you folks out there!

Content

1	Introduction	8
2	State of the art.....	10
2.1	Composition of composite materials	10
2.1.1	Polymer matrix composite (PMC)	10
2.1.2	Anisotropic behaviour of composite materials	10
2.1.3	Adhesion, critical fibre length, fibre aspect ratio and Scaling law as important factors for a stable composite.....	11
2.2	Main Components of Lignocellulose	13
2.2.1	Cellulose: the reinforcing agent.....	14
2.2.2	Hemicellulose: the glue between cellulose and lignin.....	15
2.2.3	Lignin: the supporting material	16
2.3	Thermal Modification	17
2.4	From Sugars to lactic acid, the precursor for PLA.....	18
2.4.1	Poly lactic acid (PLA)	18
3	Material & Methods	20
3.1	Polymer PLA.....	20
3.2	Fibre materials.....	20
3.2.1	Mechanical preparation of the fibre material	20
3.2.2	Solvent exchange	21
3.2.3	Drying	22
3.2.4	Grinding.....	22
3.2.5	Thermal treatment	23
3.3	Casting PLA compound film.....	23
3.4	Mechanical tensile test of the casted composite films	25
3.5	Construction of a 3D-print filament.....	26
3.6	Compounding (twice).....	26
3.7	Filament extrusion	29
3.8	Tensile test composite filament.....	29
3.9	Three point flexural test Filament.....	30
3.10	Impact Test.....	32
3.11	Melt flow rate (MVR)	32
3.12	Dynamic mechanical analysis (DMA) (Composite filament / - film).....	32
3.13	Statistical Analysis	34
4	Results	35
4.1	Fibre characterization of the different fibre specimen	35
4.2	Floating Test in chloroform	36
4.3	Qualitative microscopic and macroscopic characterization of composite films	37
4.4	Mechanical testing of composite films.....	38
4.4.1	Tensile Strength RM	38
4.4.2	Modulus of Elasticity MOE	40
4.4.3	Elongation at Break dL	41
4.5	Dynamic Mechanical Analyse composite film (DMA)	42
4.6	Characterization of the composite filament	44
4.6.1	Tensile strength	44

4.6.2	Bending Test	45
4.6.3	Impact Test.....	45
4.6.4	MVR Test.....	46
4.6.5	Dynamic Mechanical Analyse composite filament (DMA).....	46
4.7	Qualitative Microscope characterisation.....	47
5	Discussion.....	49
6	Conclusion	52
7	Bibliography	53
8	Appendix A technical data sheet matrix material	56
9	Appendix B Composite film calculation.....	57
10	Appendix C extrusion protocols	58
10.1	Compound (granulate).....	58
10.2	Filament.....	60

List of Figures

Figure 1 Left Illustration, Increase of Moe and decrease of elongation of break depending on the direction of the applied load according to the fibres, fibre (blue), composite (violet), Matrix (red); Right side decreasing stiffness (red) and tensile strength (blue) according to the load angle α ; Source: modified after [8].....	10
Figure 2 Critical fibre length, stress transferred from matrix to fibre, Source: [17].....	13
Figure 3 Particle where length, height and thickness are depending variables from length, Source: [21].....	13
Figure 4 Wood composite, a superior structure is defined by the macro and microfibrils where Lignin, Hemicellulose and cellulose is embedded; Source: modified [23].....	14
Figure 5 Chemical structure of cellobiose; Source: [25].....	14
Figure 6 Hierarchical Structure of cellulose; Source: [26]	15
Figure 7 Partial structure (top) and structure representation (bottom) of O-acetyl-4-O-methyl-glucoronxytan; Source: [25]	15
Figure 8 Chemical structures of lignin precursors: (1) p-coumaryl alcohol, (2) coniferyl alcohol, (3) sinapyl alcohol; right side dominant species in softwoods like beech; Source: modified after [25] and [23]......	16
Figure 9 Partial structure of lignin; Source: [25]	17
Figure 10 Isomeric forms of lactic acid, Source: [31]	18
Figure 11 Three main routes to from lactic acid to PLA; Source: [31], [35].....	19
Figure 12 Microfibrillation of lignocellulose fibres with Masuko Ultrafine Grinder MKCA6-2J 21	
Figure 13 Pre-grinding from Buche.....	21
Figure 14 Büchner funnel with conical flask, Source [37].....	22
Figure 15 Dried H4 (left) and CNC (right) fibres.....	22
Figure 16 H4 after grinding (left), CNC after grinding (middle), Milling machine (right)	23
Figure 17 Thermo modified Organosolve fibre, 40 min (left), 20 min (middle), 0 min (right) ..	23
Figure 18 casted composite films during drying phase	24
Figure 19 Left Picture Cutting equipment, Right Picture Composite films in vacuum oven....	24
Figure 20 Stress-Strain curve for tensile test, Source:[41]	25
Figure 21 left picture Mixing unit, right picture mixing balls with PLA and fibre sample	27
Figure 22 Extruder Collin ZK25	28
Figure 23 Left extruder Collin ZK25 with two parallel polymer strand, left Cutter Primo 100 with curvy polymer strands	29
Figure 24 descriptive build up Tensile test.....	30
Figure 25 Flexural Testing, left side 3-point bending test, left side stress distribution across the beam, Source: [44],[45]	30
Figure 26 set up bending test	31
Figure 27 Zwick/Roell HIT50P impact strength testing machine	32
Figure 28 Charpy impact Test, Source: [46]	32
Figure 29 Instron Ceast MF20, Source: [47]	32
Figure 30 Thermoplastic elastomer with crystal structure; Source:[48]	33
Figure 31 Adhesion force mapping, picture corresponding to specimen Buche, H1-H4 and MFC, Source: modified from [5].....	35
Figure 32 Average adhesion force; Source [5].....	36
Figure 33 Floating test, left side test beginning, right side after 24 hours resting time; content of the tubes beginning from the left side: H2, H1, H4, CNF, Buche, H3	36

Figure 34 Fibre distribution in the polymer films, Beginning from the left above Buche 1% below Buche 10%; MFC 1%, MFC 10%; H1 1%, H1 10%;H2 1%, H2 10%; H3 1%, H3 10%; H4 1%, H4 10%.....	37
Figure 35 Macroscopic Composite films, left side with 1% fibre and right side with 10% fibre content	38
Figure 36 Tensile Strength composite film 1[%].....	39
Figure 37 Tensile Strength composite film 10[%].....	39
Figure 38 MOE Composite films1[%].....	40
Figure 39 MOE Composite films 10[%].....	41
Figure 40 Elongation at break left side 1[%], right side 10[%] fibre load.....	41
Figure 42 DMA Composite films fibre load 1%, left side storage modulus, right side loss factor tan d	42
Figure 43 DMA Composite Films fibre load 10%, left side storage Modulus, right side loss factor tan delta	43
Figure 44 Tensile Test Composite Filament, left tensile strength, right Modulus of Elasticity	44
Figure 45 Left side Modulus of Elasticity, right side Flexural strength, below elongation at break	45
Figure 46 Impact Test	46
Figure 47 MVR test	46
Figure 48 DMA characterization composite filament, left storage modulus, right tan delta	47
Figure 49 Fibre distribution in Filament H3, MFC, H4 and Buche	48
Figure 50 Schematic representation of polymer conformation anchored on surfaces, Source: [51].....	50

List of Tables

Table 1 Comparison of adhesion interactions relative to length scale ;Source [11].....	11
Table 2 Fibre materials.....	20
Table 3 Slice distance of the grinding machine, three rounds per distance.....	21
Table 4 Solvent Polarity; modified Source: [38]	22
Table 5 Mechanical testing parameter.....	26
Table 6 3D-Filament species.....	26
Table 7 Parameter tensile test composite filament	30
Table 8 Parameter bending test	31
Table 9 Lignin content and process parameter, Source: [7].....	35
Table 10 TS 1 [%] composite films	39
Table 11 TS 10[%] composite films	39
Table 12 MOE composite films 1[%].....	40
Table 13 MOE composite films 10[%].....	41
Table 14 Estimated temperatures composite films 1 [%], storage modulus and loss factor ..	43
Table 15 Estimated temperatures composite films 10 [%], storage modulus and loss factor	44
Table 16 DMA composite filament.....	47
Table 17 Averaged Values of mechanical properties test for composite films.....	49
Table 18 Averaged Values of mechanical properties test for composite filaments.....	49

Abbreviations

%rh	Relative humidity
ABS	Acrylonitrile butadiene styrene
AFM	Atomic force microscopy
Anova	Analysis of Variance
COOH	Carboxyl group
DMA	Dynamic mechanical analysis
DP	Degree of polymerisation
FDM	Fused deposition modelling
FRP	Fibre reinforced polymer
GPa	Gigapascal
K	Kelvin
L_c	Critical fibre length
MFC	Microfibrillated cellulose
MFCL	Microfibrillated lignocellulose
MFI	Melt flow index
min.	Minutes
MOE	Modulus of elasticity
MVR	Melt flow rate
OH	Hydroxyl group
PE	Polyethylene
PEEK	Polyetheretherketone
PLA	Poly lactic acid
PMC	Polymer matrix composite
Tg	Glass transition temperature
TS	Tensile strength
Wa	Adhesion force
wt%	Weight percent

1 Introduction

“Life in plastic, it’s fantastic”-lyrics sung by the band Aqua in their Song “Barbie Girl”. Words meant it for a very famous doll, but in this short statement you can actually find an unspoken truth and an ongoing addiction from this substance for modern and highly sophisticated civilizations. It all began in the 19 th centuries with Charles Goodyear and his invention of vulcanizing natural rubber. Nowadays this natural rubber got substituted with synthetic plastics, made from fossil fuels and a world without them is unimaginable.

But what is this plastic? Plastic describes a material defined as, highly molecular organic compounds synthesized from low molecular building blocks or adapted from high molecular natural compounds [1]. A more accurate term for plastics is polymers, which is used further in this survey.

A majority of the people in the industrialized world gets more and more aware of the increasing garbage problem by a careless handling of polymers. According to Eriksen, et. al. 5 trillion particles weighing over 250.000 tons are currently floating in the sea in the size class from 0,33 [mm] to 200 [mm] [2]. The long persistence of fossil polymers is a major disadvantage and thus this small particle endangers a lot of different species, from the fish in the sea to the birds in the sky [3]. There are many biologically possible substitutes for fossil polymers available. For example bio polymers derived out of starch or other renewable resources, but the price and in some case the low mechanical properties hinders the breakthrough of these replacements. To overcome these limitations it is common practice in the industries to enhance polymers with additives, like stabilizers, plasticisers, dyes or fillers.

This leads to a material combined out of two materials, which is then called composite. This sort of material has a long history. Straw fibre for example was used to reinforce clay bricks and thus enhanced construction properties of the clay. The oldest construction is dated back 8.000 years ago and was found in Anatolia [4].

In modern times many polymers are reinforced with glass fibres, because of their good mechanical properties. But a major disadvantage is their high density and the high energy input in their production compared to natural derived fibres.

A survey conducted 2015 showed that microfibrillated cellulose (MFC) and microfibrillated lignocellulose (MFCL) are promising natural and renewable filler material to reinforce polymers instead of using artificial produced fibres [5].

One major issue in the composite construction is to improve the compatibility of these two different Materials. In the microscopic scale the polymer, called the matrix material and the reinforcing filler material have a different surface energy depending on the molecular structure. This contrary energy levels lead to bad connection ability between matrix and fibre. Hence macroscopic mechanical parameters, like tensile strength or impact strength are decreased in the composite.

A scientific work indicated, that the surface energy from lignocellulose is different compared to neat cellulose and that the lignocellulose is to be preferred over neat cellulose [6]. The physical adhesion theories are given in chapter 2 “State of the art”.

After this study a master student, of the Institute of wood technology, tried in her thesis to improve carpolactone composite films with MFCL fibre material and revealed a promising way for composite improvement. In her survey principally composite films were casted and the mechanical properties were determined [7]. In Industry thermoplastic are mainly processed via extrusion processes though. Therefore it would be interesting if the results from composite casting are transferable to this production process.

Based on these results a new investigation was issued and published by the Institute of wood technology and renewable resources in Tulln. For research, parts of this master thesis were used and following hypothesis and questions were considered to outline the problems mentioned above.

If the lignin on the MFLC changes the surface Energy there should be a measurable difference according to mechanical properties between the different fibre specimens. These mechanical properties can be increased tensile strength, Modulus of elasticity or flexural modulus. Additionally the thermal behaviour of the used thermoplastic as matrix material have to change in some way. For example, the glass transition temperature which indicates the transformation from brittle material behaviour to elastic performance should increase. Theoretically the enhanced adhesion, promoted by the lignin, should trigger an uprising internal friction between fibre and matrix.

To address these Issues, poly lactic acid was mixed with microfibrillated fibres of different origin. Additionally a part of the lignocellulose was exposed to great heat to investigate an extra hydrophobization through chemical reactions occurring during high temperature treatment.

In order to examine differences between the processes, films were casted with two different fibre loads. Afterwards mechanical tests were carried out to determine changes in the mechanical properties. Based on these results an extrusion process was carried out to construct polymer filaments for an FDM printer. Further on these filaments were characterised to see if the results were comparable to the process of the casting process.

2 State of the art

To understand the relevant parameters which influence the properties of composite material, this chapter provides an overview about the “state of the art” knowledge and physical theories.

2.1 Composition of composite materials

Composites are composed of resins, reinforcements, fillers and additives. Every single aspect plays an important role in the processing and final performance of the composite. The resin is the glue that holds the reinforcement fibre and the matrix material together. In this survey, lignocellulose served as glue between reinforcing fibre and matrix material. The cellulose on the other hand acts as a reinforcing material, because of its tremendous mechanical properties given in chapter 2.2.1.

2.1.1 Polymer matrix composite (PMC)

Fibre Reinforced Polymer (FRP) is one sort of PMC composite and is defined as a polymer (matrix), which is combined with a reinforcing material (particles, fibres, etc.). One key factor for example is the interaction in the interphase between these two materials. Furthermore fibre cross section, fibre formation and length plays an important role for the composite properties.

2.1.2 Anisotropic behaviour of composite materials

To improve the mechanical properties one key factor is the alignment of the fibres in the matrix materials. Depending on the orientation of the fibres the reinforcing ability often occurs only in several, but not in all, directions. In comparison, metal as an isotropic material has no preferred material properties direction. It shows the same mechanical properties in every direction. Figure 1 shows an aligned and ordered FRP composite. Two situations are illustrated: one shows the load in fibre direction, the other, diagonally to the fibre. The left side indicates the stress strain curve, for fibre (blue line), composite (violet line) and pure matrix (red line), in dependence on the loaded force. It is obvious, that the elongation at break (x-axis) of the pure matrix decreases but the MOE and TS increases. The opposite behaviour is observed in pure fibre.

To emphasize this behaviour, the diagram on the right illustrates the relative stiffness (red line) and tensile strength (blue line) of the fibre with increasing load angle. At an angle of 0° the stiffness and tensile strength have the maximum value [8].

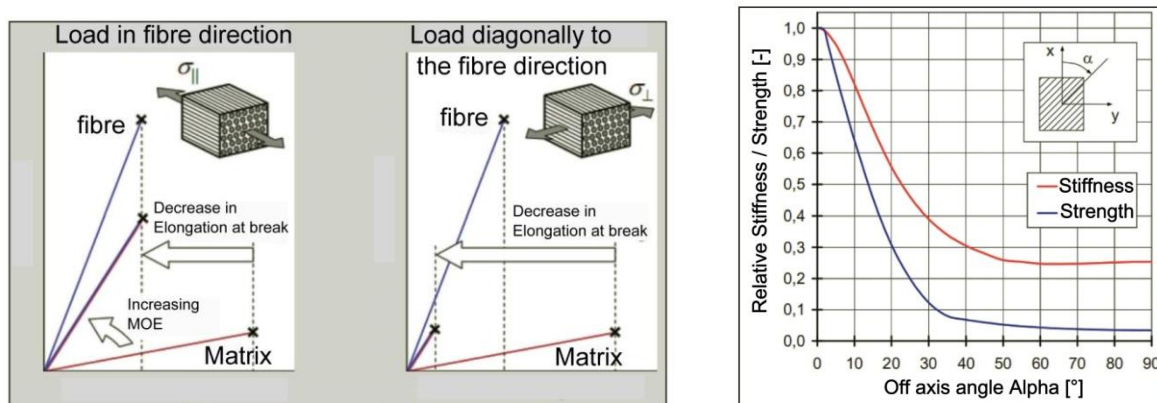


Figure 1 Left Illustration, Increase of MOE and decrease of elongation at break depending on the direction of the applied load according to the fibres, fibre (blue), composite (violet), matrix

(red); Right side decreasing stiffness (red) and tensile strength (blue) according to the load angle α ; Source: modified after [8]

The selection of composite materials depends on the intended use of the product and the stress the material has to withstand. In previous chapter 1, reasons are explained for the use of bio based polymers but for many applications the material properties, like tensile strength, have to be increased. Following list contains some benefits expected from composite materials (bold letters are properties investigated in this survey) [9]:

- **Strength**
- **Stiffness**
- Light weight
 - Therefore High strength to weight ratio
- Directional strength
- Dimensional stability
 - **Temperature dependent behaviour**
 - Thermal conductivity
- **High impact strength**
- Corrosion resistance
- Weather resistance

2.1.3 Adhesion, critical fibre length, fibre aspect ratio and Scaling law as important factors for a stable composite

Adhesion describes the interlocking or connection force between filler and matrix material. The strongest sort of fibre will fail to enhance properties of the material if it gets pulled out of the matrix during a stress situation. In literature many definitions can be found about adhesion, but for this survey it is to understand as “the molecular force of attraction in the area of contact between unlike bodies that acts to hold them together” [10].

State of the Art categorizes adhesion theories in the following seven models. Only a brief review can be given here [11]:

- Mechanical interlocking
- Electronic or electrostatic theory
- Thermodynamic adsorption or wetting theory
- Diffusion theory
- Chemical bonding theory
- Acid base theory
- Weak boundary layers theory

These mentioned theories are not stand alone theories. They are often linked together and are dependent on the length scale, in which the interfacial adhesion takes places as displayed in Table 1.

Table 1 Comparison of adhesion interactions in relation to length scale ;Source [11].

Category of Adhesion Mechanism	Type of Interaction	Length Scale
Mechanical	Interlocking or entanglement	0,01-1000 μm
Diffusion	Interlocking or entanglement	10 nm – 2 μm
Electrostatic	Charge	0,1 – 1,0 μm
Covalent bonding	Charge	0,1-0,2 nm
Acid-base interaction	Charge	0,1-0,4 nm
Lifshitz van der Waals	Charge	0,5-1,0 nm

Which theory is more suitable depends strongly on the investigated system. For example the electronic theory explains adhesion for inorganic matrices like metals, where on the other hand mechanical interlocking, diffusion and thermodynamic theories are more applicable for organic compounds [12].

According to the thermodynamic theory a high contact quality between two different materials depends on the interaction forces (van der Waals, covalent or ionic forces) and the number of contact possibilities between these materials. This can be estimated via surface energy. Thus it appears that adhesion force increases with bigger surface area which provides a higher level of interaction reactions between these two partners. The adhesion force is defined by the Dupré Equation, as needed force (W_a) when to separate two materials [13].

$$W_a = \gamma_1 + \gamma_2 - \gamma_{12}$$

γ_1 and γ_2 represent the free energy per area of the new developed surface of phase 1 and 2. γ_{12} is the specific surface energy between these two substrates.

In addition Fowkes (1987) postulated that the adhesion work can be determined as a sum of two components.

$$W_a = W_a^d + W_a^{ab}$$

W_a^d stands for the dispersive van der Waals force and W_a^{ab} for the specific interaction force of donor - acceptor interaction. Nardin proofed that for example the specific adhesion work can have a different range depending on the polarity of the matrix. He showed that in a very unpolar matrix like polyethylene (PE) the W_a^{ab} portion had 0[%] whereas in a more polar matrix such as Polyetheretherketon (PEEK) the donor acceptor interaction was about 80[%] [14]. This leads to the assumption that functional groups like hydroxyl (OH), carboxyl (COOH), benzene ring, amino-groups can act on the surface as adhesion activator, given that a contrast functional group is available[13].

De Bruyne as well interpreted adhesion through molecular, physical interactions and postulated that the two components should have the same polarity [12].

The PLA used in the survey behave more like PE with no additional donor-acceptor interactions and therefore it can be assumed that an unpolar fibre surface makes a better connection than a polar one.

Another key factor, in addition to the adhesion models, is the stress transfer from matrix material into the fibre. In a tensile loaded composite, the stress is transferred by interfacial shear stress (τ). This transferable stress increases with fibre length until the load reaches the maximal intrinsic fibre resistance. This length is called the critical fibre length L_c . Below this length L_c the fibres were pulled out in an occurring stress situation, without any remarkable stress transfers. Above this fibre length, there is no additional mechanical improvement to achieve [15]. Figure 2 illustrates the maximum stress the fibre can load. Poor compatibility between polar fibres to non-polar polymers, stress concentration occurring through micro voids and heterogeneous strain of the different phases often leads to the fact, that the intrinsic fibre resistance will not be reached [16].

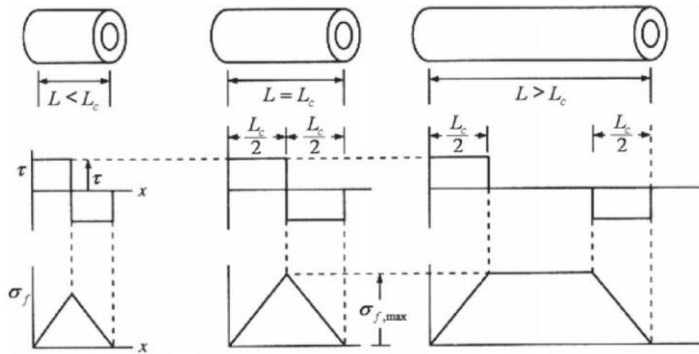


Figure 2 Critical fibre length, stress transferred from matrix to fibre, Source: [17]

There are several mathematical models, which can predict the mechanical properties of the composite like the Rule of mixture, Kelly-Tyson, Bowyer and Bader and the Cox Model [18],[19].

Additional to L_c and the physical formulas provided by the different models, a survey showed the influence of the cross-sectional aspect ratio on mechanical properties. Therefore the properties of materials of the same fibres but with different cross section shapes were estimated. The shapes varied from round until peanut butter like geometry, which as well had an impact on the properties of the composite [20].

But why is it interesting to make things smaller? A very illustrative explanation is given with scaling laws. It is a quick tool to predict changing physical properties in relation to size (Figure 3).

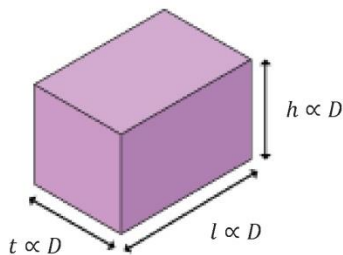


Figure 3 Particle which length, height and thickness is depending on variables from length, Source: [21]

The law for geometric parameter follows as given:

$$\text{Length} \propto D$$

$$\text{Area} \propto D^2$$

$$\text{Volume} \propto D^3$$

The specific surface area is defined as A/V and will scale therefore after the scaling law as $D^2/D^3 = 1/D$. This calculation states that with smaller size of the particle the specific surface area increases. This has an positive impact on adhesion properties as mentioned above [21].

2.2 Main Components of Lignocellulose

Cell walls of plants consist mainly of three organic compounds known as cellulose, hemicellulose and lignin. At the microscopic level these three different substances are formed as a natural composite. Lignin forms the matrix material, Hemicellulose works as a link between the matrix material and the cellulose. Figure 4 shows the hierarchical structure of the composite according to the different length scales. Further it illustrates the chemical composition, with its different sugar and phenolic building blocks [22].

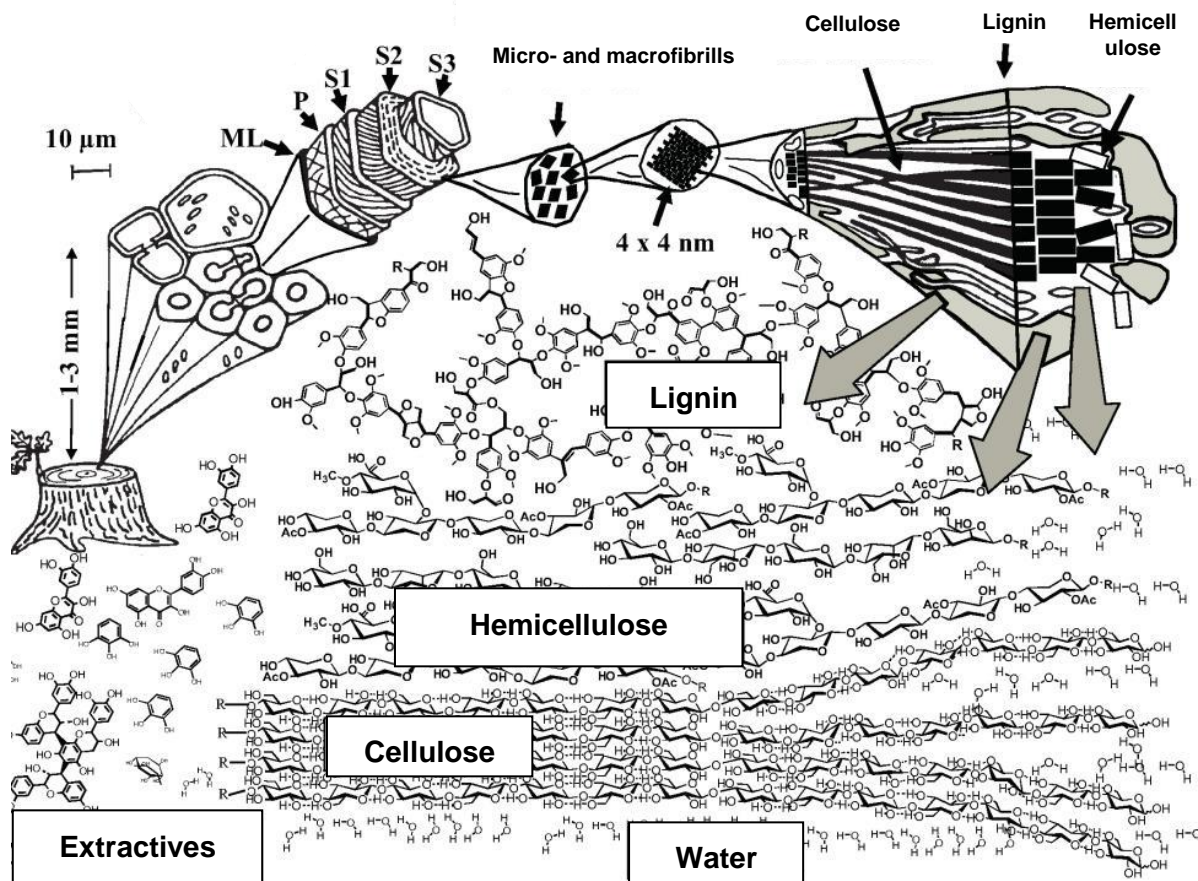


Figure 4 Wood composite, a superior structure is defined by the macro and microfibrills where Lignin, Hemicellulose and cellulose is embedded; Source: modified [23]

2.2.1 Cellulose: the reinforcing agent

Cellulose is a glucan polymer. A chemical compound of D-glucopyranose to be precise, which is mainly derived out of linked β -(1-4) Glucopyranose units called cellobiose (Figure 5). The repeating units of the polymer consist of these two-sugar units. With a total quantity on earth of 10^{11} tons, cellulose is the most abundant polymer on earth [24].

The degree of polymerisation (DP) refers to the cellulose molecule units. Cellulose has an average DP of 9.000 – to 10.000 but can have up to 15.000 units. An Average DP of 10.000 would correspond to a linear chain length of up to 5 μ m [25].

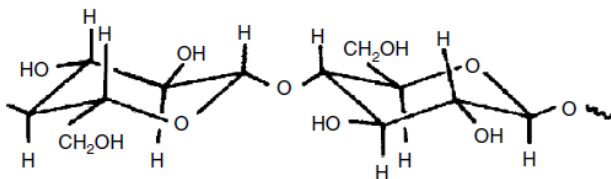


Figure 5 Chemical structure of cellobiose; Source: [25]

Cellulose has the tendency to form intra- and intermolecular hydrogen bonds. Through this behaviour the packing tendency of cellulose increases and crystalline regions can be formed

[25]. Referring back to Figure 4 it shows how tight the cellulose is packed, compared to lignin and hemicellulose. Cellulose has a strong hierarchical structure reaching from micro- to macro fibrils as illustrated in Figure 6. Hence it provides high tensile strength. Thus, for a perfect crystalline structure, several authors calculated, a Modulus of Elasticity (MOE) from 130 to 250 [GPa] and a tensile strength from 0,8 – 10 [GPa] [24]. A major drawback in the use of cellulose in polymer matrices is their high polarity tracing back to their high amount of hydroxyl (-OH) groups. Furthermore its (-OH) groups on the backbone can absorb water molecules, which leads to a swelling of the fibres and therefore influences the properties of the composite.

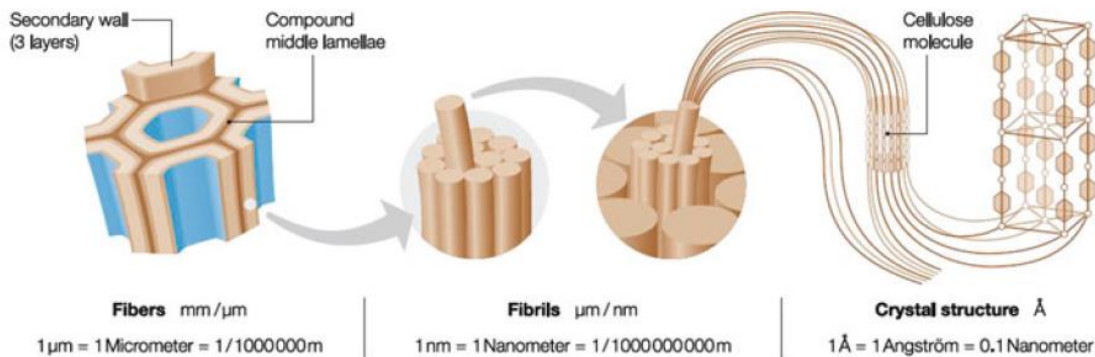


Figure 6 Hierarchical Structure of cellulose; Source: [26]

2.2.2 Hemicellulose: the glue between cellulose and lignin

In comparison to cellulose, hemicellulose (also known as polyose) has a huge variety on the molecular level. It consists of several polysaccharides like anhydrous hexose (e.g. glucose same component as in cellulose, mannose, Galactose etc.) and anhydrous pentoses (e.g. Xylose, Arabinose etc.). The acidified form of these sugars can also be found in hemicellulose such as glucuronic acid or galacturonic acid. To simplify the family of hemicelluloses they can be classified as xylanes and glucomannan [23].

Hemicelluloses usually consist of more than one type of these sugar units. Figure 7 shows a representative of these classes (O-acetyl-4-O-methyl-glucuronxyylan). The backbone consists mainly of xylan units, whereas glucuronic acid units occur in the branch.

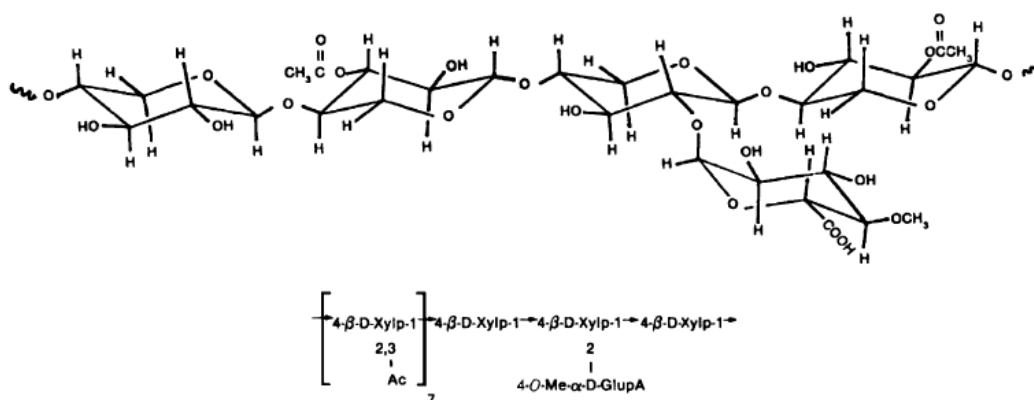


Figure 7 Partial structure (top) and structure representation (bottom) of O-acetyl-4-O-methyl-glucuronxyylan; Source: [25]

This huge variability and their occurring side branches lead to a very low DP in comparison to cellulose (DP < 1000). In pure state, hemicelluloses are amorphous and not crystalline, also mainly caused to the appearance of their side chains. In a pure state, hemicelluloses are amorphous rather than crystalline, which is mainly caused by the appearance of their

side chains. These compounds lack hydroxyl (OH) groups and therefore can't form hydrogen bonds in the same intensity as the cellulose. [23].

2.2.3 Lignin: the supporting material

Lignin is a highly complex compound and is mainly build up from aromatic polymers derived out of phenylpropane units, which are considered as an encrusting substance. The three dimensional structure is mainly made up of C-O-C and C-C linkages between these phenyl propane units, but there can be also some side linkages on the aromatic ring. This ultimately leads to a very complex structure that is not fully comprehended at this time.

The precursor substances shown on the left side in Figure 8 are p-coumaryl alcohol, coniferyl alcohol and sinapyl alcohol. The first species structure (1) is a minor precursor in the wood cell wall, where species (2) and (3) are predominately found in the different wood types [25]. Their occurring ratio is strongly dependent on whether it is a hardwood, softwood or even lignified grasses. The GS lignin on the right side of Figure 8 is the dominate species of lignin in softwood, like the beech wood used in the survey and it has additional methoxy groups (-OCH₃) on the aromatic ring. These groups promote the poor reactivity and their unpolar behaviour of the compound [23].

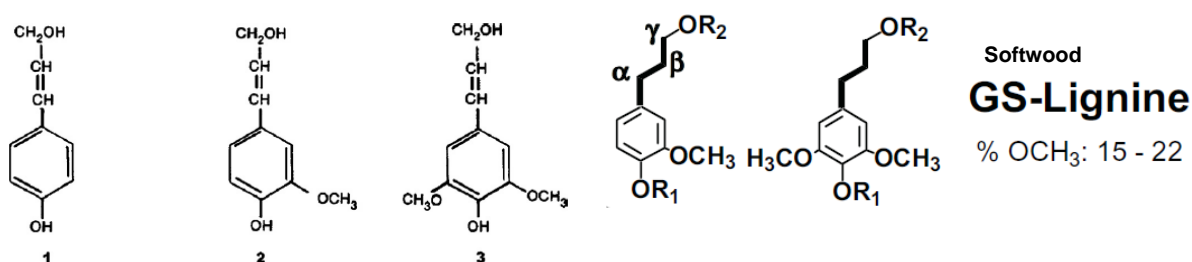


Figure 8 Chemical structures of lignin precursors: (1) p-coumaryl alcohol, (2) coniferyl alcohol, (3) sinapyl alcohol; right side dominant species in softwoods such as beech; Source: modified after [25] and [23].

Figure 9 illustrates a partial structure of lignin and their way they link in several different ways. It shows the single phenolic precursor units and their ability to arrange as a macro molecule, which is strongly dependent on the existence of the single precursor units. Through their different coupling reactions they form a highly complex polymer [25].

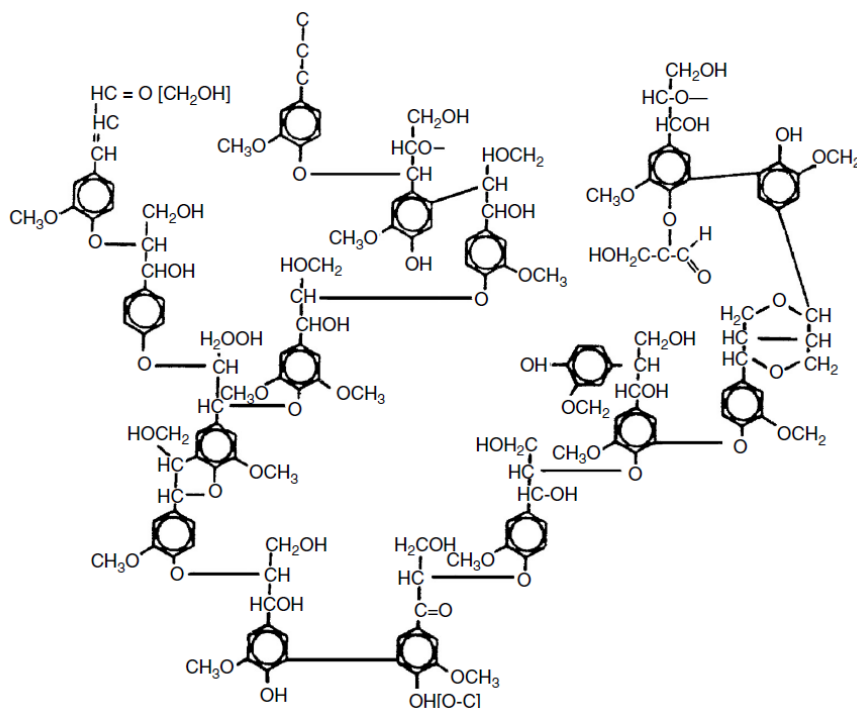


Figure 9 Partial structure of lignin; Source: [25]

In comparison to pure cellulose with its abundance of (-OH) groups, the lignin structure leads to a more evenly distributed electron cloud, particularly generated by their aromatic rings. According to de Bruyne (compare 2.1.3), this more evenly distributed polarity should lead to a better interaction between reinforcement fibre and matrix material.

2.3 Thermal Modification

The first thermal wood modification, to improve dimensional stability, was reported by Tieman in 1915. By treating the wood with high temperatures the water absorption rate could be reduced. The reduced hygroscopicity indicates an increased unpolar behaviour of the wood substances and thus an improved merge into the polymer matrix is expected.

Thermal modifications are performed between 180 [°C] to 260 [°C]. At temperatures lower than 140 [°C] only slightly changes occurs in the wood properties. Whereas by treatment temperature above 300 [°C] a high degradation takes place in the substrate [27].

The onset temperature for hemicellulose degradation begins at 100 [°C] [28], forming acetic acid and various volatile heterocyclic compounds. Fengel and Wegener report a degradation of the DP at 100 [°C] for isolated cellulose. In general though, literature describes the beginning of degradation at higher temperature. Kim (et. al.) investigated decomposition of crystalline cellulose above 300 [°C] [29]. Chemical transformations occur in the complex Lignin substrate below 200 [°C]. Above this temperature lignin begins to degrade.

As a result of the thermally induced modification following alterations of properties are determined [30]:

- Dimensional stability
- Reduced hygroscopicity
- Higher resistance against microbiological attack
- Reduction of impact toughness, flexural strength and work to fracture
- Reduced abrasion resistance
- Darkening of the material

Although the fibre structure itself loses mechanical properties to degradation by the thermal treatment, the improvement of adhesion forces could outweigh this factor.

2.4 From Sugars to lactic acid, the precursor for PLA

Lactic acid occurs naturally in microorganisms and is part of many fermented products like butter, yoghurt, sour dough bread, etc.. So it is a metabolic process in which glucose and other six carbon sugars are converted into cellular energy and the metabolite lactate. Renewable sources are mainly corn starch (United States and Canada), tapioca roots, starch or sugarcane. The chemical compound is shown in Figure 11 in its two isomeric constitutions.

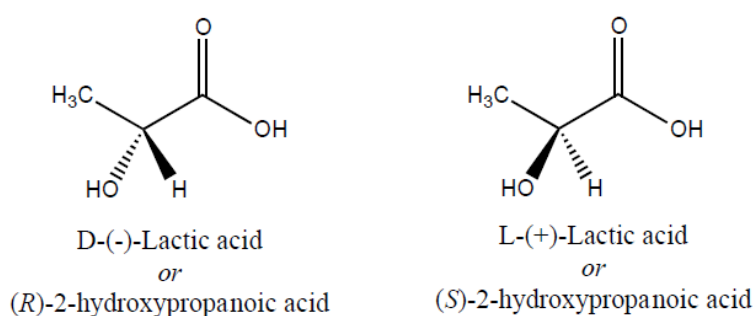


Figure 10 Isomeric forms of lactic acid, Source: [31]

Lactic acid can be produced in a petrochemical pathway, through hydrolyses from lacto nitrile. Today 95% of the worldwide production is based on a fermentative pathway using lactobacillus species bacteria [32]. These fermentation processes can be quantified according to the type of bacteria used. Firstly the heterofermentative pathway, which produces lactic acid besides other compounds like acetic acid, ethanol, carbon dioxide or glycerol. Secondly the homo-fermentative pathway, which leads to greater yields of lactic acid and lower levels of by products [33].

The Advantage of this procedure is the easy adjusting of produced D, L or mixed isomers (racemic). This regulation is very important in the view of the next production step, forming a polymer. For good material properties it is important that the resource base for poly lactic acid is build-up of one type of isomers [34].

2.4.1 Poly lactic acid (PLA)

PLA is an aliphatic polyester which is composed out of lactic acid monomers as previously described. It is a semi crystalline Polymer constructed from single lactic acid building blocks [1].

The synthetic rout is shown in Figure 11. Three possible main routes are known through polycondensation from low molecular oligomers, azeotropic dehydrative condensation or ring-opening polymerization from the dilactid. The first route leads to brittle and low molecular polymers which need further coupling agents to increase its chain length. The ring opening and the dehydrative condensation way leads to high molecular PLA [35].

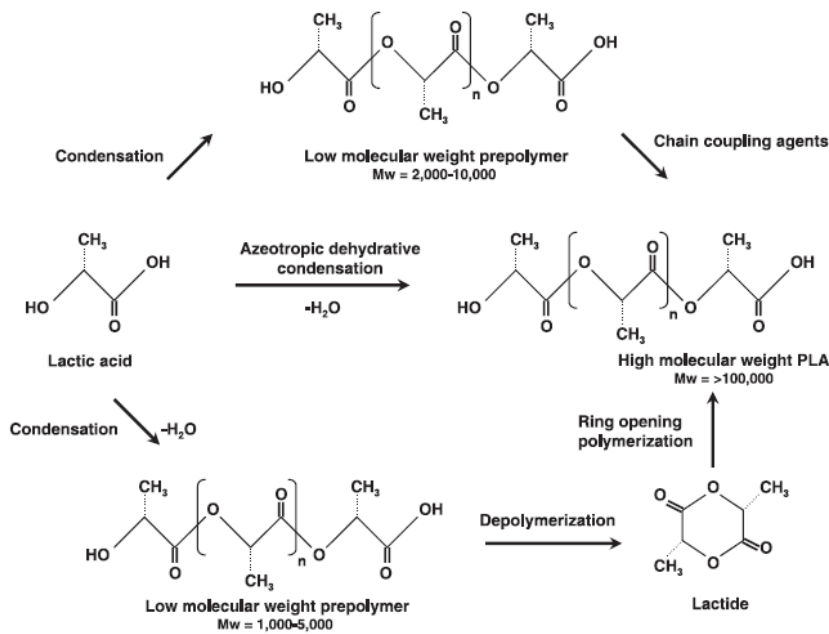


Figure 11 Three main routes from lactic acid to PLA; Source: [31], [35]

Because of its biodegradability PLA is utilized for disposable products like forks, cups, bottles and plates. Additionally it can be used for textile or as suture material in medicinal applications [1].

PLA is characterized by the following properties[1]:

- Semi crystalline thermoplastic (for details see chapter 3.12)
- Resistance against alcohol, moist and fat
- Rigid and flexible, depending on the modification
- Shiny, transparent surface
- Dyeable
- Addition of fillers possible

3 Material & Methods

Following chapter lists the experimental methods and the required Materials for the investigation. The required fibres and their individual properties and modification before being used in the composites are described first. Afterwards the execution of the mechanical and thermal testing will be explained more detailed.

3.1 Polymer PLA

The used Polymer was obtained from Cargill Dow LCC (Minnetonka, Minnesota, USA). The trading name of the product was NatureWorks PLA polymer 4043D and it was delivered in pellet form. The melting point was at 145 – 160 [°C] with a density of 1,24 [g/cm³] and it had a Melt Index of 20 [cm³/10min] which was determined in 3.11. Additional information is available in the technical data sheet at Appendix A, chapter 8.

3.2 Fibre materials

Table 2 shows the fibre materials and their individual treatments carried out on them by a organosolv process from the University of Hamburg [7]. The fibre specimens can be distinguished in process time and the concentration by supplied H₂SO₄. Additional to these specimens, the table shows the untreated fibre and the thermal treated fibre samples, separated by the double line in the table. For the investigation approximately 36 g of dry mass was used per specimen.

Table 2 Fibre materials

Name	Revealing temperature	Pressure	H ₂ SO ₄	Process time
H1	170°	15bar	0%	90min
H2	170°	15bar	0,25%	90min
H3	170°	15bar	0,75%	90min
H4	170°	15bar	0%	60min
Buche	This is the source material for H1 – H4			
MFC	Pure cellulose material from the University of Main			
Name	Remarks			
H1 _{Tt}	Thermal modified fibres			
H2 _{Tt}				
H3 _{Tt}				
H4 _{Tt}				
Buche _{Tt}				
MFC _{Tt}				

3.2.1 Mechanical preparation of the fibre material

In order to gain microfibrillated lignocellulose, the samples H1 to H4 were mechanically treated by the grinding machine Masuko (Saitamaken, Japan) - ultrafine grinder MKCA6-2J (Figure 12). Therefore the fibres were diluted in deionized water to 1.5-2 [wt%] and stored in the refrigerator at 7 [°C] for one week. Storing the fibre led to a swelling of the material which simplified the subsequent step of mechanical crushing. All runs were performed at the

same speed of 1500 [rev/min] and were carried out three times per slice distance. The applied slice distances are illustrated in Table 3.

Table 3 Slice distance of the grinding machine, three rounds per distance

Slice Distance [mm], starting with the first row from the left		
0.4	0.15	0.02
0.35	0.10	0.00
0.30	0.08	-0.02
0.25	0.06	-0.04
0.20	0.04	-0.06



Figure 12 Microfibrillation of lignocellulose fibres with Masuko Ultrafine Grinder MKCA6-2J



Figure 13 Pre-grinding from Buche

The Buche Material was stored in the cold room at -18 [°C]. It was then thawed and diluted in deionised water to 1 [wt%]. As a next step the material was pre-grinded using a merchantable 450 [W] hand held blender (Braun, Germany) (Figure 13). Additionally it was mechanically crushed in the same way as the organosolv material in Table 3.

The MFC fibres had already been fibrillated by University of Main and therefore further grinding wouldn't have had any effects on the particle size.

3.2.2 Solvent exchange

Before the fibres could be mixed into the dissolved PLA solution, they had to be dried completely. Directly out of water dried cellulosic material become a very hard bulk, because of their agglomeration behaviour induced during the drying process [36]. Yucheng (2011) showed that under these circumstances, the cellulose forms strong intermolecular hydrogen bonds and builds a strong fibre network.

To prevent the occurring of this agglomeration, the fibres diluted in water were transferred in two different organic solvent. The idea was to influence the drying properties of the fibre by shifting the solvent polarity step by step from a more polar into an unpolar solvent. The individual polarity values are shown in Table 4.

First the fibre samples were washed with ethanol three times and afterwards in isopropanol for another three times. In every washing step the fibre suspension was stored in the solvent for a minimum time of thirty minutes. The washing was performed by a 5 litre Büchner funnel

with a 10 [μm] filter paper fitted on a conical flask connected with a Vacuum pump as illustrated in Figure 14.

It should be noted that there are many different ways to characterise the polarity of solvents and many different indicators were developed over time. But they should be considered as a benchmark that helps to classify them. Table 4 shows the excluded table of the different polarisation behaviour of solvents and their physical properties, as used in this work. $E_t(30)$ represents the solvent polarity parameter in [kJ/mol]. Water has the highest value in the table compared to the other organic solvents.

Table 4 Solvent Polarity; modified Source: [38]

Solvent	Melting point. [$^{\circ}\text{C}$]	Boilingp. [$^{\circ}\text{C}$]	density [g/cm^3] bei 20 C	$E_t(30)$ [kJ/mol]
Ethanol	-114,5	78,3	0,7893	216,9
2-Propanol	-89,5	82,3	0,7855	203,1
Water	0	100	0,9982	263,8



Figure 14 Büchner funnel with conical flask, Source [37]

3.2.3 Drying

To get a dry powder the fibre suspension in the isopropanol solution was stored in a drying oven of the type Memmert UF30. The drying was carried out under a fume hood for 8 hours at 90 [$^{\circ}\text{C}$] and at a fan power of 80 [%].



Figure 15 Dried H4 (left) and MFC (right) fibres

As shown in Figure 15, the dried fibres tend to build soft, but bulky agglomeration which needed further mechanical treatment.

3.2.4 Grinding

After drying, the fibres were grinded using an IKA MF 10 basic milling machine. The milling speed was 5000 [rev/min] and the sieve width used was 0.5 [mm]. During this grinding step roughly 11 [%] of the dry mass was lost during the grinding process per specimen.



Figure 16 H4 after grinding (left), MFC after grinding (middle), Milling machine (right)

Figure 16 shows the fibre species after the grinding process in the milling machine. Compared to the fibres in Figure 15 the material got less bulky and fleecier. This simplified the further steps of mixing the fibre into the dissolved polymer/chloroform solution.

3.2.5 Thermal treatment

After the mechanical treatment, the fibres were split up in two equal amounts of dry mass. The browning process was taken as an Indicator for the chemical transformation explained in chapter 2.3. To determine the perfect time, a pre-test was started. Figure 17 shows the three different heat treatment stages. The Petri dish on the left contains the sample with 40 minutes treatment, the one on the right shows a sample untreated fibre (0 min.). In the middle there is a 20 minutes treated fibre with slightly changed colour.

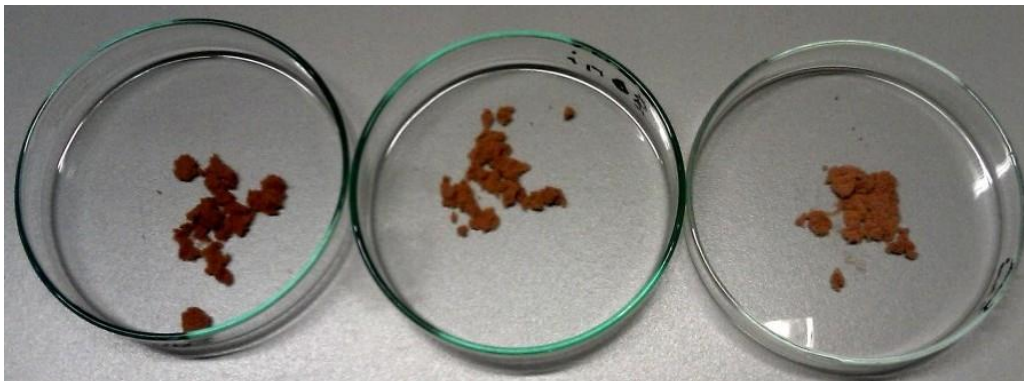


Figure 17 Thermal modified organosolv fibres, 40 min (left), 20 min (middle), 0 min (right)

For the survey thermal modification was done in a drying oven by 200 °C with a fan power of 80% at 40 minutes.

3.3 Casting PLA compound film

The PLA was dissolved in Chloroform at a ratio of 1:20 for a minimum of 7 hours and stored in a dark bottle with additional parafilm sealing at the screw cap. Chloroform tends to undergo a photochemical reaction under the influence of light and oxygen and transforms into toxic phosgene (COCl_2) compound [39].

The PLA/Chloroform suspension was mixed with the different fibre species. Composite films were casted with a fibre load of 1[w%] and 10[w%]. To achieve a constant film thickness of 0.1 [mm] the PLA/Fibre suspension were calculated after the formula listed in the appendix, chapter 9.

Before the cast was started, a scale and the Petri dishes were put under the fume hood. Because of the toxicity and the low steam pressure of chloroform each of the following steps

was performed under the fume hood. Before the fibres were mixed with the PLA suspension, they were dried for two hours in a Memmert UF30 drying oven at 103 [°C] and the calculated dry mass was weighed on an analytical balance. Afterwards the PLA suspension and the fibres were filled in a 100 [ml] Erlenmeyer flask and mixed for 2 minutes using an Ika Ultra Turrax Dispenser. A single Petri dish was put on the scale and the balance was tared. The PLA/fibre suspension was casted on the Petri dish and the process was stopped at the correct calculated mass. The mass on the scale was changing very fast during the casting process, because of the low steam pressure and the venting from the fume hood, which additionally increased the evaporation rate of the chloroform solution. To achieve a satisfying result this step had to be carried out very quickly.

The filled Petri dishes were stored under the fume hood and during the drying phase they were covered with cleaning paper as illustrated in Figure 18. The drying took about sixteen hours at a temperature of approx. 21 [°C] and a fume hood fan power of 600 [m³/h].

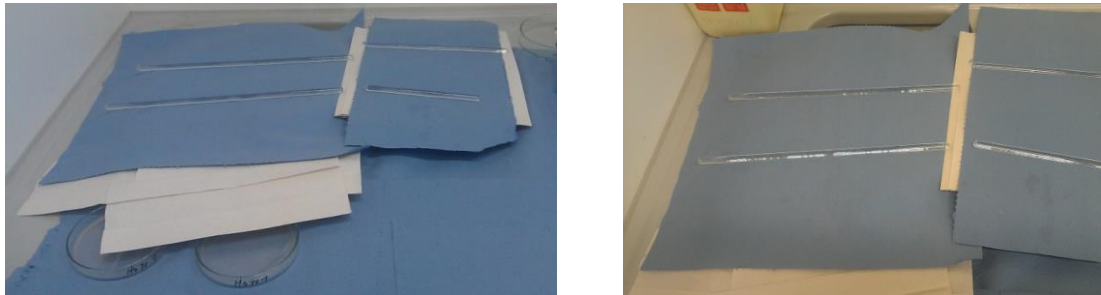


Figure 18 casted composite films during drying phase

After drying, the films were cut out of the Petri dishes with a sharp knife and were put in a vacuum oven type VO 400 by Memmert GmbH (Figure 19). Before testing the composite films, it is important that all of the residual solvent in the composite films is evaporated. Remaining solvent in the composite film can lead to falsely investigated mechanical properties like reduced E Modulus or increasing elongation at break. In order to prevent this from happening, the films were additionally dried at a temperature of 40 [°C] and by low pressure of 80 [mbar] for half an hour. This should lead to a full evaporation of remaining solvent but as shown in chapter 4.4 a few composite species held odd results by elongation at break. Therefore a longer drying time and higher temperature can be recommended.



Figure 19 Left picture cutting equipment, right picture composite films in vacuum oven

3.4 Mechanical tensile test of the casted composite films

The variation of strain with stress that is obtained from a tensile test produces a stress-strain curve (Figure 20). According to Hooke's law, the slope of the elastic Region determines the Modulus of Elasticity (MOE). The onset of the nonlinear curve occurs when the deformation of the material changes from elastic (reversible) to plastic (irreversible) behaviour. Furthermore it shows the maximum stress the material can withstand and the maximum elongation, before the material breaks apart. The maximum stress and the elongation point is very similar in brittle materials, whereas in rubber like material the curve can have a very different shape with exhibiting a distinctively plastic region illustrated on the right side of Figure 20. Other properties obtained from this curve are ductility, toughness and resilience [40].

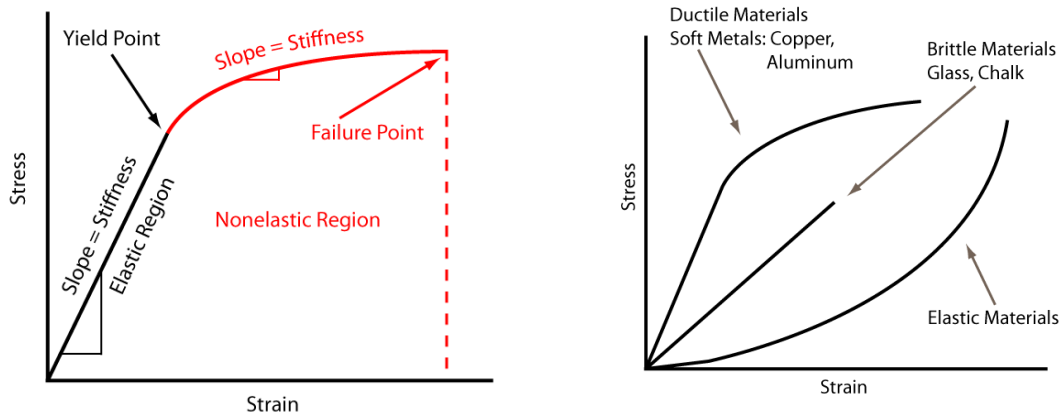


Figure 20 Stress-Strain curve for tensile test, Source:[41]

For the mechanical characterization the composite samples were cut in a geometry of 50x8 [mm] and conditioned at a humidity of 46 [%] and a Temperature of 21 [°C] for 2 hours in the testing room. The tensile tests were accomplished with a Zwick/Roell Z100. It was equipped with a 500 [N] force measuring socket and a special carrier for thin composite films. The deformation was measured using a contact type extensometer BZ2-EXI55000A.1XXX from the Zwick/Roell Company. The data were evaluated with the testXpert II -V3.5 program.

Following properties got evaluated:

- Tensile strength [N/mm²]
- Elastic modulus [GPa]
- Elongation until break [%]

The parameters for testing were adjusted as shown in Table 5 Mechanical testing parameter.

Table 5 Mechanical testing parameter

Parameter name	Setting
Threshold of power switched off	80% F max
Testing speed	10 mm/min
E Modulus	Type: Regression Start 3 MPa End 6 MPa
Free clamping length	30 mm
Measuring length standard way (extensometer)	16 mm

3.5 Construction of a 3D-print filament

Based on the mechanical tests on the composite films the amount of different specimen types was reduced. Following sample categories were chosen for the extrusion, illustrated in Table 6. The processed total mass was about 1690 [g] with 1% fibre load per sample. First step was to compound a granule with an extruder. The PLA was then mixed with the fibres. In the second step the 3D-Print filament got extruded by the same extruder but different Parameter setting.

Table 6 3D-Filament species

Name	Remarks
H1	1 % Fibre and 99 % PLA 4043D content, without thermal treatment
H2	
H3	
H4	
MFC	
Buche	

3.6 Compounding (twice)

For compounding preparation, the purchased PLA 4043D was grinded using a type SM1 by Retsch GmbH milling machine with a 2 [mm] sieve. Afterwards the PLA was dried at 70[°C] in the drying oven for 16 hours. Before processing the fibre material was dried at 120[°C] for 16 hours as well. The material had to be as dry as possible to prevent water evaporation during the extrusion, because the compounder had no gasification section. If it had such a section, the excess water from the polymer or fibres could evaporate. This is very crucial for PLA extrusion, because this sort of polymer can be autocatalytically hydrolyzed by interaction with water at high temperature. Thus, the polymerisation grade decreases and mechanical properties worsen.

The following devices were needed for the compounding process:

- Metering Unit (Figure 22)
- Extruder (Figure 22)
- 2 Conveyor belts (Figure 23)
- Granulate cutter (Figure 23)

PLA and fibre were put in a 50 l bucket at a dispersal of 99 to 1. Afterwards three hands full of mixing balls with a diameter from 4 [cm] were filled in the bucket and it got sealed. The bucket was fixed in a mixing unit of the type “RRM Elte 650” by the Engelsmann AG and rotated in the machine for a minimum of 15 minutes as illustrated by Figure 21.



Figure 21 left picture mixing unit, right picture mixing balls with PLA and fibre sample

The compounding was carried out using a Collin ZK25 opposite parallel double screw extruder (Figure 22). A higher throughput of the material at shorter residence time is the advantage of this system compared to a single screw extruder. The time to heat up the extruder was 30 to 45 min for reaching the correct temperature of the single zones. The temperatures in the single zone were, T1 (120 °C), T2 (165 °C), T3 (165 °C) and the temperature at the compounding tool was set at T (160 °C). The compounding tool had two outlets with a diameter of 3 [mm]. The rotation speed of the extrusion screw was 65 rpm.

After the mixing process, the material was filled in the metering Unit of the type 3327P from the K-tron company and the speed was set to 260-300 [rpm/poti]. The feeding speed depended strongly on the situation during the extrusion process. The speed was adjusted to prevent the material from backing up in the hopper zone. The aim was to establish a continuous flow from metering unit to the extruder. The set parameters and single remarks to the different samples can be looked up in the Appendix under chapter 10.1.



Figure 22 Extruder Collin ZK25

At the beginning of the process and after every specimen extrusion the hopper was filled with neat PLA and the screw was swept through with it. This cleared the extrusion channels from residues.

At the beginning, approx. four grams were taken from the process and the humidity got measured with a HS 153 Moisture Analyzer by Mettler Toledo. The determined moisture value was about 0.09%.

The compounded strand was directed to a double conveyor belt system. Each conveyor belt had a length of 2 meters. There were no marks for the regulation of the conveyor belt speed. The regulation of the speed was adjusted over the haul of speed occurring in the extrusion tool. This speed strongly determined the strand diameter. If the diameter ranged between 2.75 - 2.95 [cm], the haul off speed was considered to be correct.

After the first 2 meters the polymer cooled down under standard environmental conditions without any additional cooling system. The second conveyor belt speed was lower than the first and was adjusted to the cutter speed. For the process, a cutter of the type Primo 100 by Rieter Company was used. The entering speed was set to 10 [rpm/min]. That was the lowest possible speed achieved by this machine and despite of the setting, in some cases to quick. Figure 23 shows the process and emphasizes the two different conveyor belt speeds through the curving of the filament on the right picture.



Figure 23 Left extruder Collin ZK25 with two parallel polymer strands, left Cutter Primo 100 with curvy polymer strands

The granules from the cutter were stored in a bucket situated directly under the machine. When the material was finished the whole granulate got compounded **a second time** with no changing in the procedure.

3.7 Filament extrusion

Before filament extrusion, the granules were stored for 16 hours over night in the drying oven at 90 [°C]. After drying, the material was very sticky and was separated by hand. The process was comparable to the one in chapter 3.6. The rotation speed from the extrusion screw was changed to 35 [rpm] and thus the metering unit speed changed to 180 [rpm/poti]. As well the speed of the conveyor belt was adjusted to the new circumstances. The Temperature in the different zones was set to T1 (150 °C), T2 (178 °C), T3 (178 °C) and a tool temp.(160 °C) as shown in Figure 22. The protocols for each individual filament extrusion can be seen in the appendix under 10.2 for every sample. After the extrusion, the individual filament was rolled up to separate bundles and stored in the storage room at 21 [°C] and 60 [%rh].

3.8 Tensile test composite filament

The filament composites were tested on a Zwick/Roell Z020 universal testing machine (Figure 24). Each testing samples were individually cut in 8 [cm] long pieces. The diameter of the filament differed from 2,64 to 2,95 [mm]. The samples were conditioned in the testing room for 2 hours at 21 [%rh] and 46 [%rh].



Figure 24 descriptive build up Tensile test

Evaluated Parameters:

- Modulus of Elasticity [GPa]
- Maximum Force [MPa]
- Elasticity at Maximum Force [%]

Table 7 Parameter tensile test composite filament

Parameter name	Setting
Threshold of power switch off	80% F max
Testing speed	10 mm/min
E Modulus	Type: Regression Start 15 % Fmax End 25% Fmax
Free clamping length	50 mm

3.9 Three point flexural test Filament

Similar to the tensile test, the applied load of the material produces a stress strain curve and provides a modulus of elasticity in bending, flexural stress and flexural strain. Most common types of tests are 3 point (Figure 25) and 4 point bending test. In the survey a 3 point test method was used. The difference compared to a tensile test is, that a flexure test does not measure fundamental material properties. Under the testing situation combined effect in the specimen occurs of tensile, compressive and shear forces [42]. Not only cross section area, as in the tensile test plays a major role, also the shape of this area has a strong impact on the measured value. Flexural strength is defined as the maximum stress at the outermost layer where the stress has its maximum load (Figure 25). The flexural modulus is calculated from the slope of the stress to its strain curve [43].

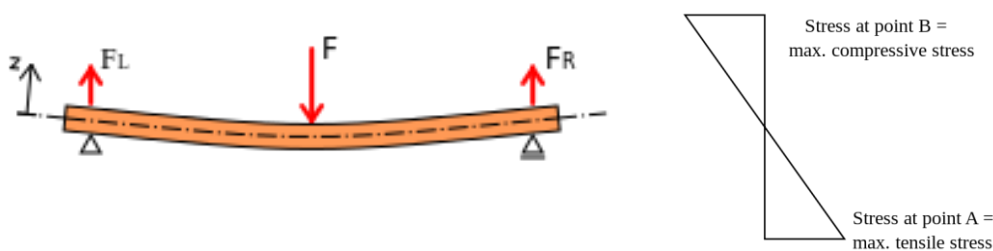


Figure 25 Flexural Testing, left side 3-point bending test, right side stress distribution across the beam, Source: [44],[45]

The characterisations of the different filament specimens were performed using a three point testing method on a Zwick/Roell Z020 universal testing machine. Before testing, the material was stored for several weeks in the storage room at 21°C and 60[%rh]. Before testing the material was conditioned in the Testing room at 21 °C and 46[%rh] for two hours. The different filaments were cut into 6 [cm] long samples and the diameters were measured at three different positions.

Following parameters were evaluated:

- Modulus of Elasticity [GPa]
- Maximum force [MPa]
- Deformation at maximum force [%]
- Deformation at break [%]

Table 8 shows the adjusted parameter and Figure 26 illustrates the set up for the bending test. It should be emphasized that the single specimen were lightly curved, because the whole filament was stored rolled up.

Table 8 Parameter bending test

Parameter name	Setting
Tool distance in starting position	3,00 [mm]
Testing speed	100 [mm/min]
Speed Elastic Modulus	Position control 25 [mm/min]
Testing end	Max. Temporal power loss 5 [n/mm ²] Upper force threshold 500 [N] Max. Deformation 50 [mm]
Bending characteristics	Pad roll radius 12,5 [mm] Radius bending stamp 13,5 [mm]
Distance between supports	24 [mm]

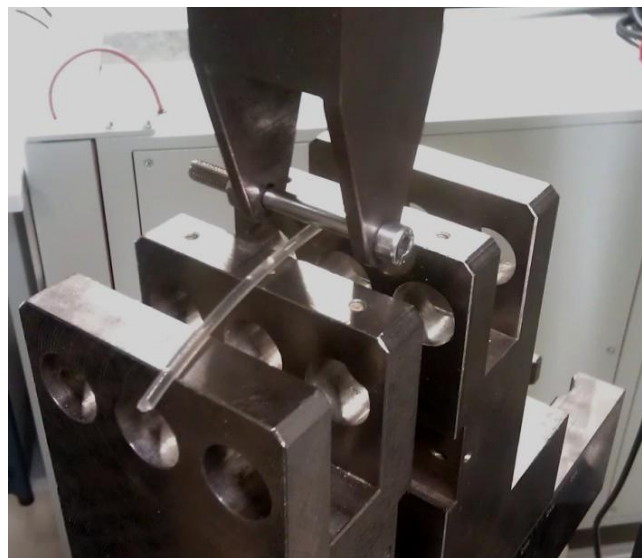


Figure 26 set up bending test

3.10 Impact Test

The fracture toughness can be measured by an impact test. This test measures how much energy is needed to cause a fracture of the material by a known dimension. The absorbed energy is determined through the difference between the potential energy in starting position and on the first reversal point. The standard testing method is the Charpy impact test and the test set up is illustrated in Figure 28 [40].

The determination of the impact strength was carried out using a Zwick/Roell HIT50P. The testing samples were conditioned for 24 [h] at 21 [°C] and 46 [%rh]. Five samples of every specimen were taken. The impact Pendulum was equipped with 5[J] hammer. The measured energy absorption was calculated using the diameter and the impact strength. Figure 27 shows the testing machine HIT50P.



Figure 27 Zwick/Roell HIT50P impact strength testing machine

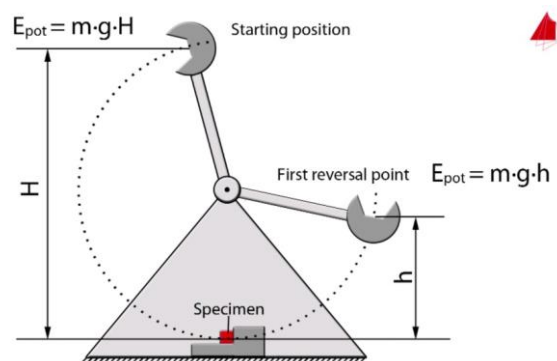


Figure 28 Charpy impact test, Source: [46]

3.11 Melt flow rate (MVR)

The melt flow rate test is a simple method of characterizing the flow properties of a melted polymer mass and is a standard procedure in the Industry for quality control. The MVR was measured after the standard ISO 1133 F by an Instron Ceast MF20, illustrated in Figure 29. The testing weight was 10 [kg] and the procedure was performed at 190 [°C] with a preheating time of 240 [s]. Two samples were tested for every composite type.



Figure 29 Instron Ceast MF20, Source: [47]

3.12 Dynamic mechanical analysis (DMA) (Composite filament / - film)

For polymers not only mechanical tests are interesting, also the changing material properties in different thermal conditions can lead to a deeper understanding of the structure.

dependant on the flexural modulus, the diameter was transferred and calculated based on the same flexural modulus as a squared diameter. Following equations were used:

$$W_{ax} = \frac{\pi x D^3}{32} \text{ flexural moment round diameter}$$

$$W_{sq} = \frac{a^3}{6} \text{ flexural moment squared diameter}$$

$$a = \sqrt[3]{\frac{6x\pi}{32} x D^3} \text{ equivalent length for the programm}$$

Film composite:

The thin films were tested via tensile test. The samples of the films had a rectangular shape of 6x20 [mm]. Two test samples were prepared per specimen. The Measurements were carried out at a constant frequency of 5 [Hz] and the temperature range was from 20 [°C] to 120 [°C].

Dynamical Parameters were set as followed:

- Constant statical force 0,1 N
- Dynamical force 4,364 N
- Force factor 1,1
- Amplitude 15 μm

3.13 Statistical Analysis

The data were statistically analysed by an Analysis of variance (ANOVA) to evaluate if there is any significant deviation between the samples. Because the ANOVA model only describes a global occurring variance a post hoc test "Tukey's test" was chosen to investigate the difference between the single composite specimens. A 5% level of significance was chosen.

4 Results

4.1 Fibre characterization of the different fibre specimen

The biology institute in Hamburg measured the lignin content of the treated beech samples in a two stage hydrolysis process. Table 9 shows the lignin content in dependency on the used process parameter.

Table 9 Lignin content and process parameter, Source: [7]

Species	Time [min.]	Temperature °C	H2SO4/Wood atro [%]	Lignin content [%]
H1	90	170	0	12,43
H2	90	170	0,25	9,38
H3	90	170	0,75	4,37
H4	60	170	0	13,46
Buche	0	0	0	22,2

Evidently, with an increasing amount of H₂SO₄, the lignin content H2 and H3 dropped rapidly. In comparison to the treatment time, the decrease of Lignin is not so severe.

Additionally to the chemical analysis, the fibre adhesion force was characterized via Atomic force microscopy (AFM). The single specimens are illustrated in Figure 31. With a distribution ranging from 1 nN to 75 nN, the specimen H4 showed the highest variability in adhesion force [5].

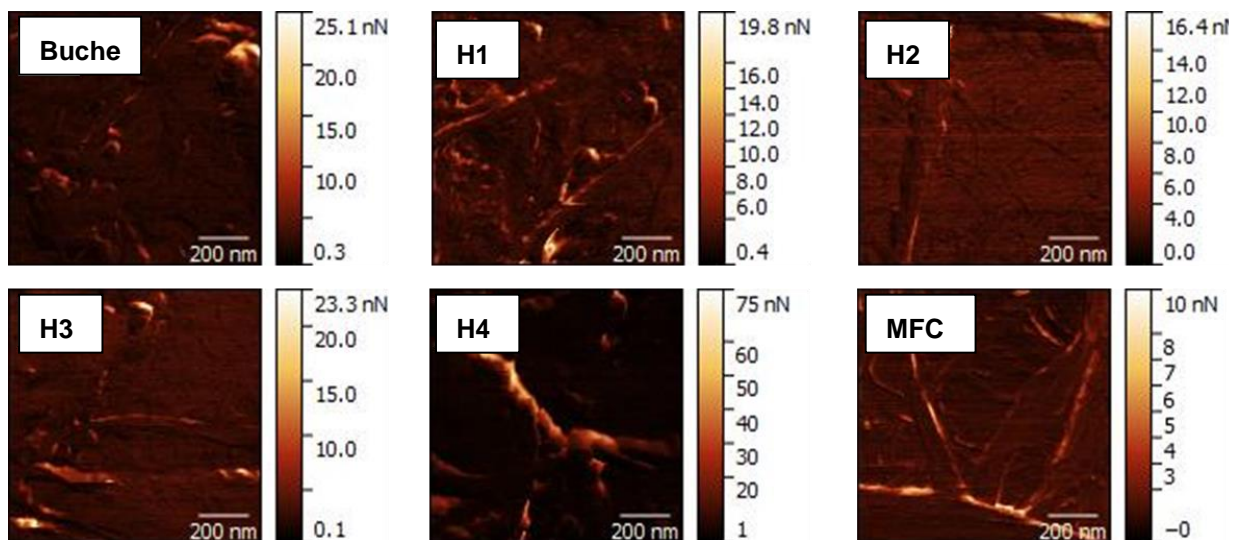


Figure 31 Adhesion force mapping, picture corresponding to specimen Buche, H1-H4 and MFC, Source: modified from [5]

Figure 32 provides more information by illustrating the average adhesion force of the single specimen. All lignocellulosic fibres have overall a wider distribution and a stronger adhesion force than pure MFC fibres. The narrow distribution of the MFC fibres results from its more unified chemical compilation. This corresponds to the theoretical illustration of cellulose like as presented in chapter 2.2.1.

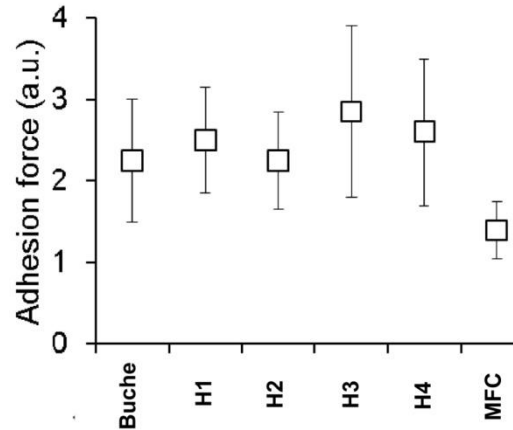


Figure 32 Average adhesion force; Source modified after [5]

4.2 Floating Test in chloroform

The floating test is a fast test to investigate the miscibility of solids with a solvent. If the two components are very similar in their polarity there will be no precipitation. It will rather be a homogeneous dispersion. Figure 33 shows the floating test carried out in chloroform with 1 wt% fibre content. The left side shows the fibre after shaking. The different specimens are distributed well inside every tube. The right side shows the same specimen after 24 hours resting time. It is clear to see that precipitation occurred in H2, Buche and H3, which indicates an aversion of these specimens to the unpolar solvent.

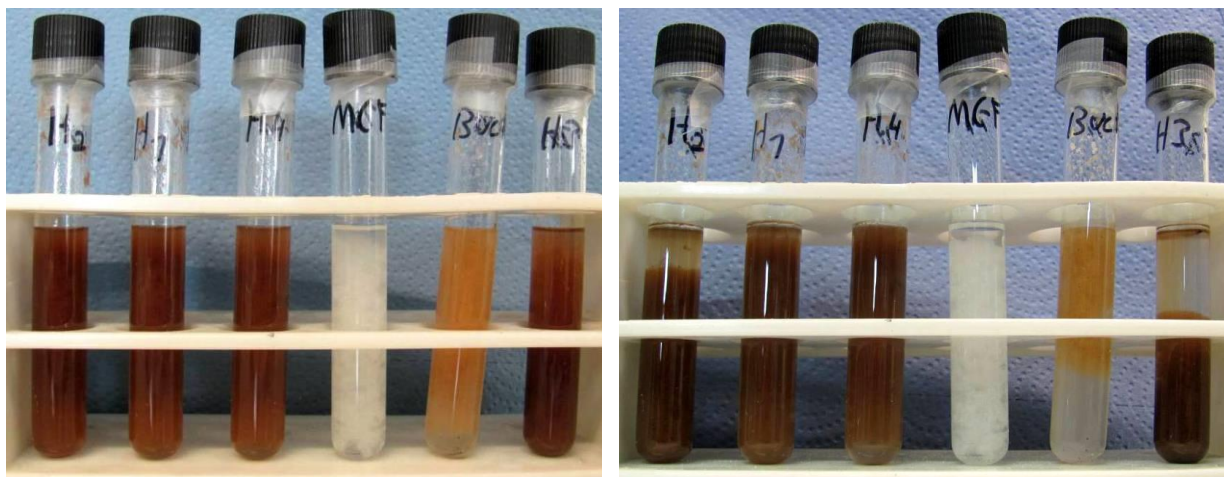


Figure 33 Floating test, left side test beginning, right side after 24 hours resting time; content of the tubes beginning from the left side: H2, H1, H4, MFC, Buche, and H3

The testing tube containing the Buche specimen was showing a peculiar behavior. Other than H2 and H3, this one floated upwards even though the density of the fibre should be similar and higher than the density of the solvent. Also the MFC result was unexpected. Despite the fact that it is a very polar component, no precipitation occurred.

4.3 Qualitative microscopic and macroscopic characterization of composite films

The pictures illustrated in Figure 34 show the distribution of the fibres in the polymer matrix. The red line on the right bottom corner indicates the width of 1 [mm].

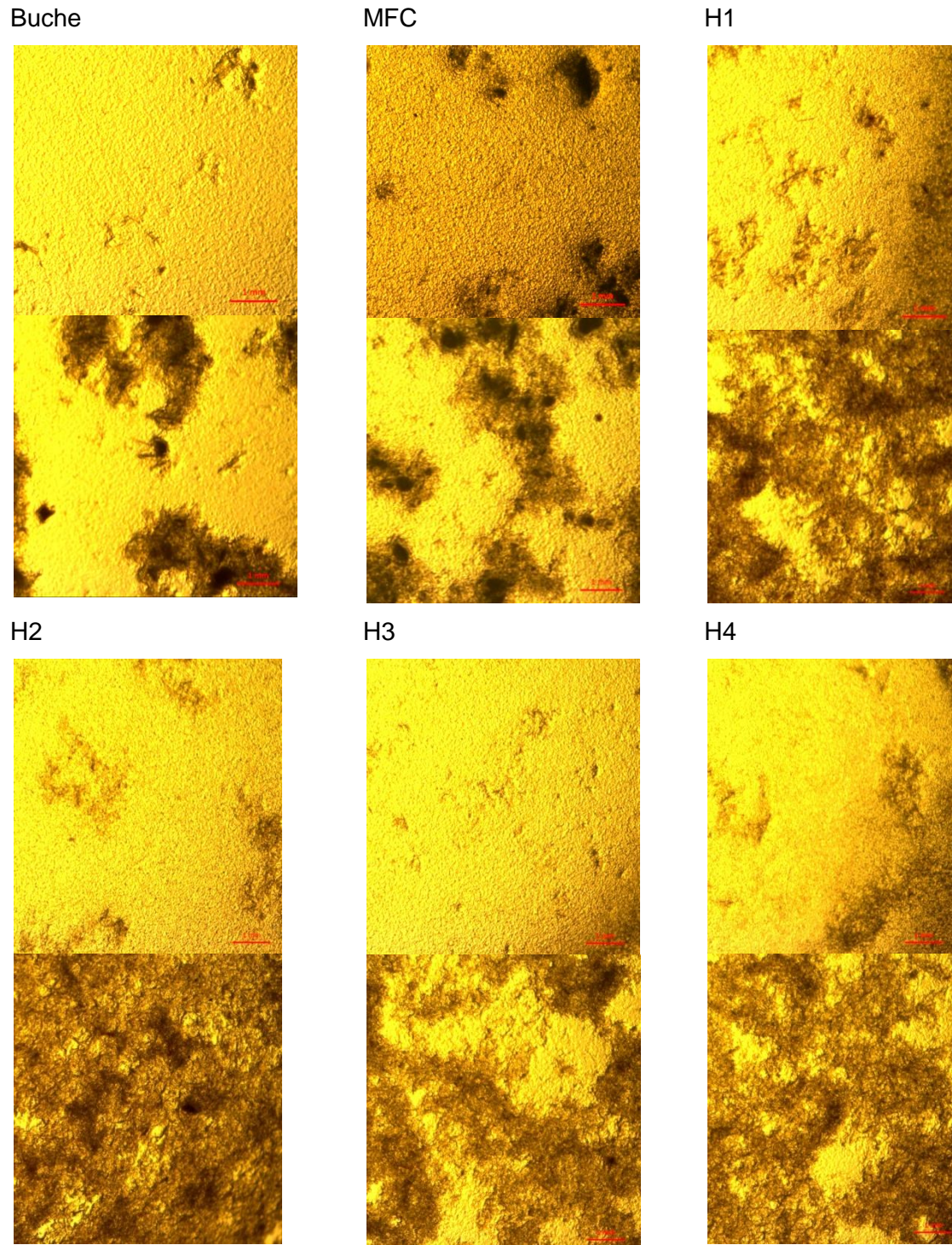


Figure 34 Fibre distribution in the polymer films, Beginning from the left above Buche 1% below Buche 10%; MFC 1%, MFC 10%; H1 1%, H1 10%; H2 1%, H2 10%; H3 1%, H3 10%; H4 1%, H4 10%

In Buche and MFC 10 % the fibres packed very tightly to closed compartments. Also in the section of MFC 1%, very dense and dark bulky fibre areas can be clearly seen. In the other specimen, the distribution area broadens in comparison to the Buche and MFC specimen but very clear coagulation of the fibre can be seen in every specimen. Especially in the 10% fibre load films the distribution of the specimens H1 – H4 is far better than compared with the MFC or Buche samples.

Figure 35 shows the macroscopic composite film H2 with 1% and 10 % fibre content. Especially in the specimen with 1% the organization of small fibre islands was observed during the drying phase. These islands rapidly formed after the casting process. The sample containing 10% fibre load seemed as if they had better fibre dispersion but when measuring the thickness, it showed that this composite film had irregular film thickness and thus showing agglomeration zones as well.

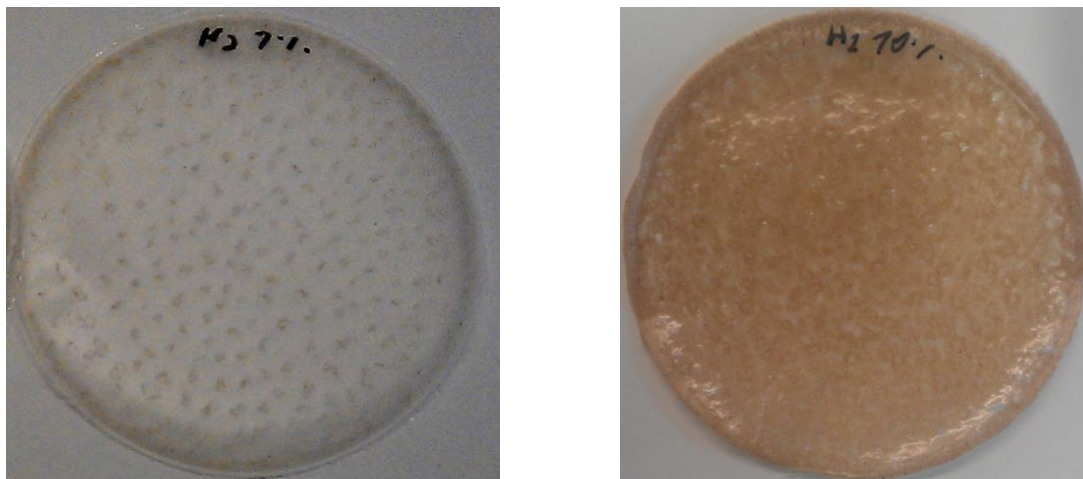


Figure 35 Macroscopic Composite films, left side with 1% fibre and right side with 10% fibre content

4.4 Mechanical testing of composite films

This chapter shows the results of the mechanical testing, as explained in chapter 3.4.

4.4.1 Tensile Strength RM

Figure 36 shows the tensile strength (TS) in [N/mm²] according to the different specimens. In addition Table 10 shows the mean values of the estimated TS values with their standard deviation and the occurring difference compared to pure PLA. Overall every sample with 1% fibre load increased in TS of the matrix material, except the specimen of the untreated wood fibres B1 and B1Tt. The specimens H3, PLA and MFC were highlighted to emphasize the behaviour of lignocellulosic reinforcement fibre in comparison to neat cellulose and the pure matrix material. Bearing in mind Table 2 and Figure 32, it is very interesting that the fibre sample with the roughest organosolv treatment but with the highest adhesion force showed the best performance. The thermal modification and the theoretical hydrophobization discussed in chapter 2.3, didn't show a significant effect on the mechanical properties compared to the untreated fibre specimen. The difference between the thermal modified fibres in comparison to the untreated fibres was in the range of the occurring variance.

The statistical analysis showed a positive Levene Test and a significant distinction between the specimens with an R² of 0,44. There was a significant difference between the single highlighted specimens (H3 to PLA and the MFC samples) according to Tukey's test.

Table 10 TS 1 [%] composite films

Specimen	Mean value [N/mm ²]	Std. Devi.	Diff [%]
B 1%	25.287	1.09	-6
BTt 1%	26.062	0.69	-3
H1 1%	32.189	1.88	19
H1Tt 1%	34.161	2.60	27
H2 1%	27.427	2.31	2
H2Tt 1%	29.341	4.78	9
H3 1%	34.651	2.62	28
H3Tt 1%	31.394	5.79	16
H4 1%	30.098	1.92	11
H4Tt 1%	28.549	2.47	6
MFC 1%	29.846	4.09	11
MFCTt 1%	32.509	2.57	20
PLA	27.001	0.82	-

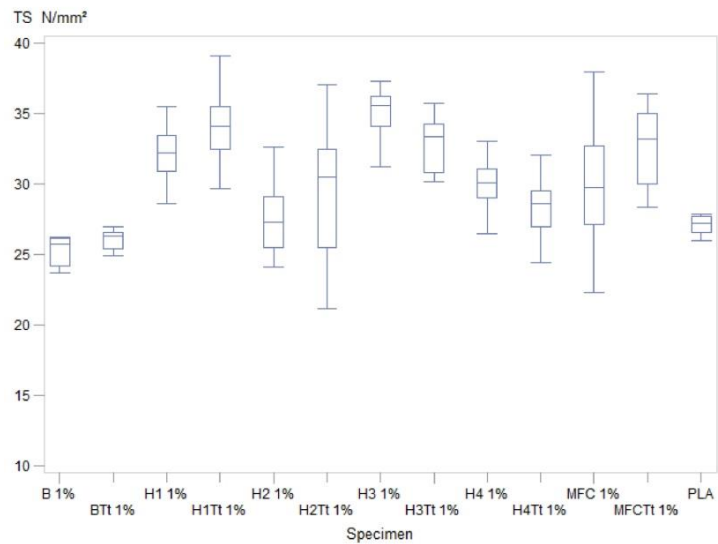


Figure 36 Tensile Strength composite film 1[%]

Table 11 lists the composite films with 10 [%] fibre loads and their respective mean values, standard deviation and the difference according to neat PLA, additionally illustrated in Figure 37. Generally all samples with 10 [%] fibre load led to a reduction of the TS in the range from -27[%] to -40[%]. This indicates a bad dispersion of the fibres with the bulk matrix material. Also the H3 sample showed a worse performance compared to the sample with 1[%] fibre load.

The statistical analysis for the TS showed a significant variation in the data set. The R² was 0,84 and thus the model could explain 84 [%] of the occurring variance.

Table 11 TS 10[%] composite films

Specimen	Mean value [N/mm ²]	Std. Devi.	Diff [%]
B 10%	16.352	1.72	-39
BTt 10%	13.483	3.50	-50
H1 10%	17.338	2.80	-36
H1Tt 10%	19.798	1.75	-27
H2 10%	12.584	3.31	-53
H2Tt 10%	11.486	1.32	-57
H3 10%	17.341	3.52	-36
H3Tt 10%	11.739	1.71	-57
H4 10%	18.296	2.76	-32
H4Tt 10%	14.813	1.27	-45
MFC 10%	16.083	2.89	-40
MFCTt 10%	16.094	2.23	-40
PLA	27.001	0.82	-

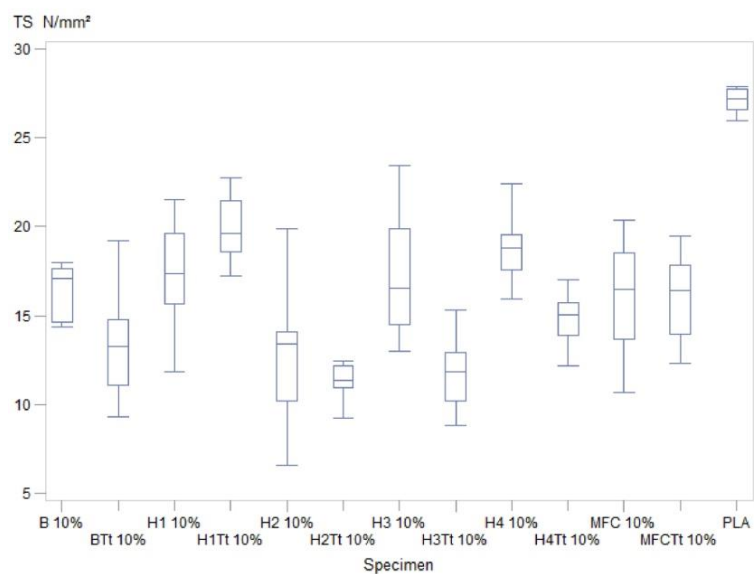


Figure 37 Tensile Strength composite film 10[%]

4.4.2 Modulus of Elasticity MOE

Figure 38 displays the different composite film specimens with 1 [%] fibre load according to their Modulus of Elasticity (MOE), whereas Table 12 summarizes the mean values, standard deviations and appearing differences compared to neat PLA. In general the 1[%] fibre load samples had a higher MOE, except for B1 and BTt1. The sample with the best performance was H3 with an additional improvement of 37 [%] to neat PLA and 5-18 [%] higher value than the composite containing MFC fibres.

Table 12 MOE composite films 1[%]

Specimen	Mean value [GPa]	Std. Dev.	Diff [%]
B 1%	0.872	0.04	-3
BTt 1%	0.909	0.04	1
H1 1%	1.153	0.09	28
H1Tt 1%	1.171	0.10	30
H2 1%	0.995	0.11	10
H2Tt 1%	1.043	0.15	16
H3 1%	1.233	0.05	37
H3Tt 1%	1.194	0.07	32
H4 1%	1.077	0.07	19
H4Tt 1%	1.101	0.10	22
MFC 1%	1.075	0.13	19
MFCTt 1%	1.188	0.08	32
PLA	0.903	0.06	-

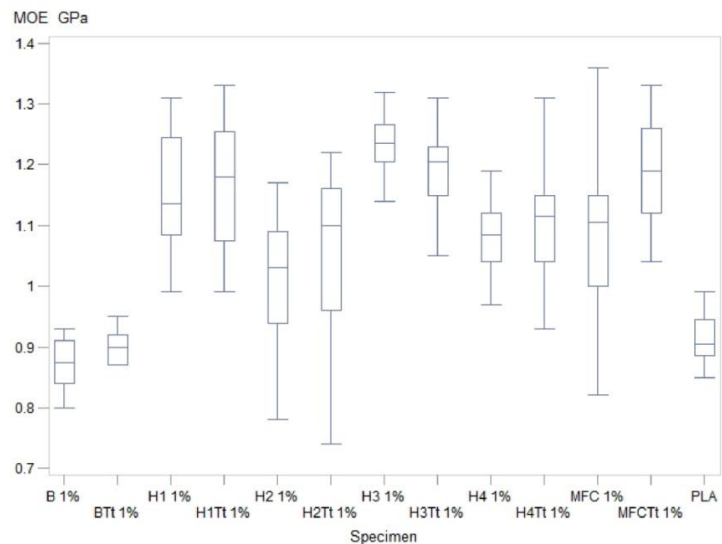


Figure 38 MOE Composite films 1[%]

Figure 39 and Table 13 summarize the measured values from the 10[%] fibre load samples. Specimens weakened the compound up to -48 [%] in the worse case.

Table 13 MOE composite films 10[%]

Specimen	Mean value [GPA]	Std. Dev.	Diff [%]
B 10%	0,61	0.12	-32
BTt 10%	0,52	0.14	-42
H1 10%	0,79	0.11	-12
H1Tt 10%	0,90	0.08	0
H2 10%	0,57	0.11	-37
H2Tt 10%	0,47	0.06	-48
H3 10%	0,74	0.18	-18
H3Tt 10%	0,50	0.07	-44
H4 10%	0,81	0.13	-10
H4Tt 10%	0,66	0.08	-27
MFC 10%	0,61	0.12	-32
MFCTt 10%	0,69	0.11	-23
PLA	0,90	0.06	0

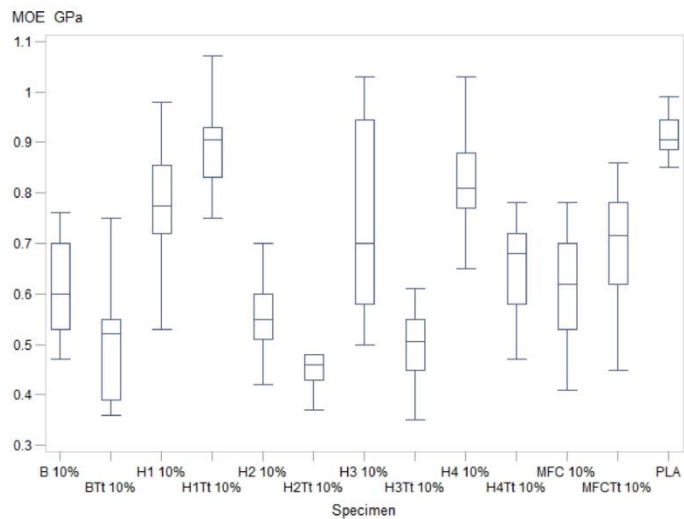


Figure 39 MOE Composite films 10[%]

The statistical analysis for the Moe showed a significant variation in the data set. The R^2 was 0,84 and thus the model could explain 84 [%] of the occurring variance. The comparison with the Post hoc test calculated, that H3 with 1[%] fibre load had a significant different to all other specimen, especially to MFC 1[%] fibre content and neat PLA.

4.4.3 Elongation at Break dL

According to Figure 40 there is a tremendous variability in the samples B1, H4Tt and PLA. This could be due to solvent residues in the polymer Matrix, leading to an additional gain of elastic behaviour. Therefore the time of the drying process should be increased to several hours, compare to chapter 3.3. Nevertheless an additional fibre load reduces the elongation at break. Overall, an increase of fibre content from 1% to 10% indicates a tremendous decrease of elongation abilities of the matrix material.

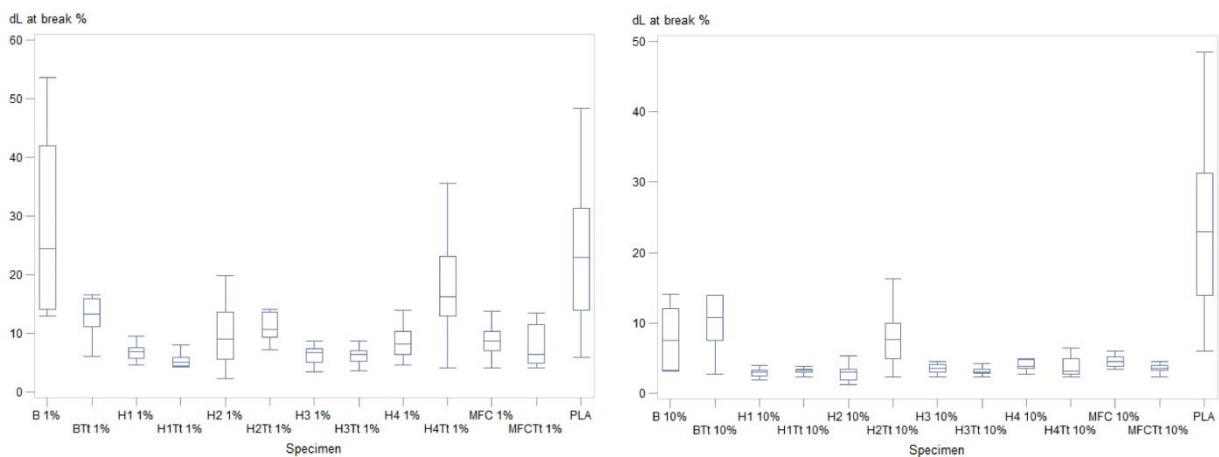


Figure 40 Elongation at break left side 1[%], right side 10[%] fibre load

The statistical analysis shows a significant variation according to the p value with an R^2 of 0,56.

4.5 Dynamic Mechanical Analyse composite film (DMA)

All the mechanical tests showed that the thermal modification had no significant impact on the composite. Thus for the DMA Analyses only non-thermal modified samples were tested.

The performance of the DMA Analysis is displayed by Figure 41 for the 1[%] fibre load and Figure 42 for the 10[%] fibre load in comparison with the neat PLA. The test was performed until 100 [°C] to measure a change in the glass transition (T_g) temperature. The samples start at different storage modulus where the specimen H4 has the highest rate with 2600 [MPa] and H2 the lowest with 1402 [MPa]. The storage modulus decreased during the rising of the temperature which indicated the transition from its brittle state to its elastic state. To determine the range of the T_g temperature there are two possibilities. First is to choose the turning point of the storage modulus, second one to use the highest point at the curve by the loss factor tan d.

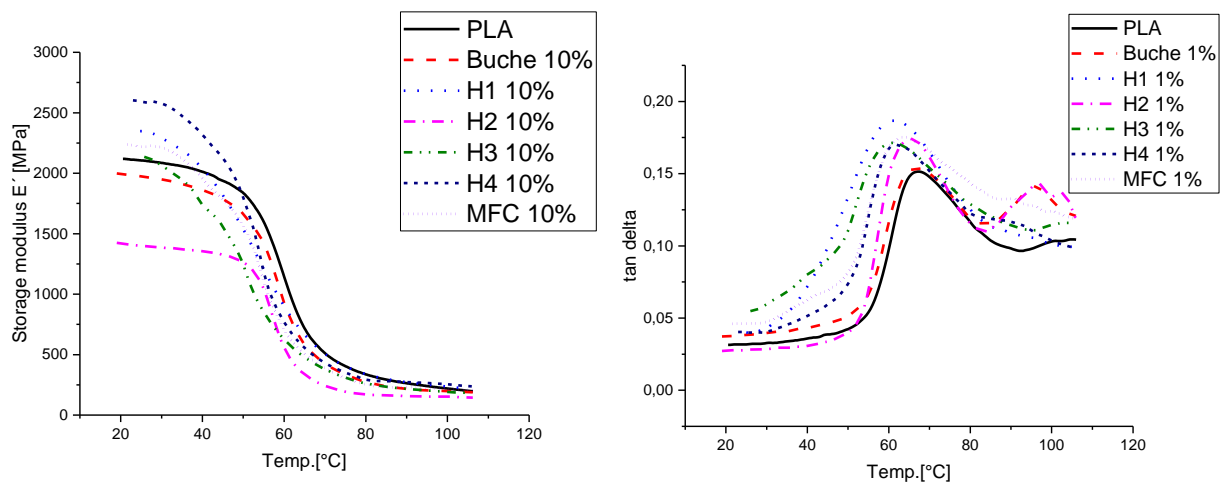


Figure 41 DMA Composite films fibre load 1%, left side storage modulus, right side loss factor tan d

Table 14 lists the different temperatures of the DMA measurement. It shows, that the difference between the turning point of the storage modulus and the peak point of tan d is about 10 [K]. Looking at the data, neat PLA had the highest T_g temperature rate ranging from 59,4 [°C] to 67,1 [°C]. In comparison the specimen H3 with the best mechanical performance had a T_g range from 51,9 [°C] to 61,3 [°C] whereas the specimen Buche with low quality mechanical performance had a higher T_g range, similar to neat PLA of 58,1 [°C] to 67,1 [°C]. According to a survey by Huda et. al., a reduction of the tan delta peak is due to the immobilization of polymer matrix in the presence of the fibres [49]. Considering the tan delta graph, PLA has the lowest peak compared with the fibre loaded samples, which as well can indicated a bad adhesion between fibre and matrix, although the mechanical properties were improved.

From this point of view, the different specimen showed similar viscoelastic properties and there was no indication that the microfibrillated fibres had a positive influence of the thermal stability on the neat PLA.

Table 14 Estimated temperatures composite films 1 [%], storage modulus and loss factor

Specimen 1[%]	Temp at turning point E` Storage Modulus [°C]	Temp. at peak point from tan d [°C]
H1	54,4	61,3
H2	56,7	65,4
H3	51,9	61,3
H4	54,0	61,4
MFC	54,3	63,9
Buche	58,1	67,1
PLA	59,4	67,1

Figure 42 shows the DMA measurement of the 10% fibre load specimens. Apparently they started with a very low Storage Modulus ranging from 500 [MPa] (Buche 10%) to 1400 [MPa] compared to neat PLA with 2100 [MPa] or the samples containing 1 [%] fibre.

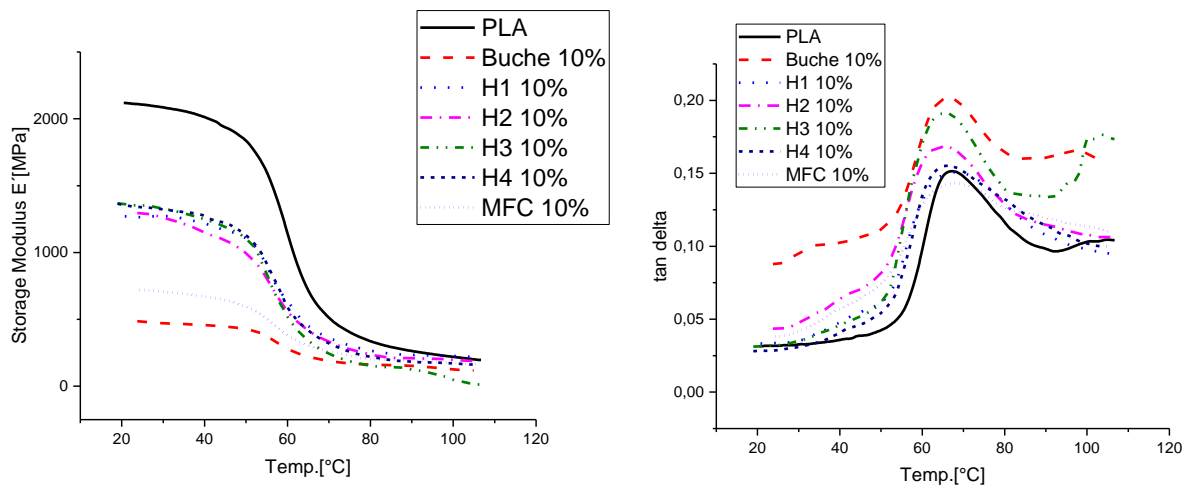


Figure 42 DMA Composite Films fibre load 10%, left side storage Modulus, right side loss factor tan delta

Table 15 shows, similar to the table containing 1 [%] fibre load specimens, that the differences between the Tg temperature comparing the storage modulus with the loss factor tan delta is approx. 10 [K]. As well in the specimen with 10 [%] the fibre load didn't increase the Tg value compared to the neat PLA specimen.

Table 15 Estimated temperatures composite films 10 [%], storage modulus and loss factor

Specimen 10[%]	Temp at turning point E` Storage Modulus [°C]	Temp. at peak point from tan d [°C]
H1	56,1	68,1
H2	56,2	65,3
H3	54,7	65,3
H4	55,9	66,0
MFC	57,1	67,9
Buche	56,6	66,2
PLA	59,4	67,1

4.6 Characterization of the composite filament

This chapter provides data about the results of the mechanical and thermal characterisation of the composite filament.

4.6.1 Tensile strength

In comparison to the casted composites, the tensile test of the filament showed a different behaviour. Looking at Figure 43, the best performing material was the neat PLA with an MOE, in the Median of 2.9 [GPa] and a tensile strength of 59,8 [MPa]. Every sample with a fibre load of 1[%] gave a worse performance. It is to emphasize, that the theoretically more polar components like pure Cellulose and untreated wood fibre showed a better performance than the treated fibres. Other than stated in chapter 3.4 the specimen H3 had an additional increase of tensile strength compared to neat PLA and MFC fibres. This effect cannot be detected after filament extrusion, which could indicate that the blending in the in the mixing unit was not sufficient and the merging in the extruder was ineffective. The data shows, that the distribution of the fibre was insufficient and the additional adhesion force owing by unpolar region and therefore, was too weak to increase the mechanical properties. Also the decrease in the MOE exhibits a weakening effect due to the fibre loading.

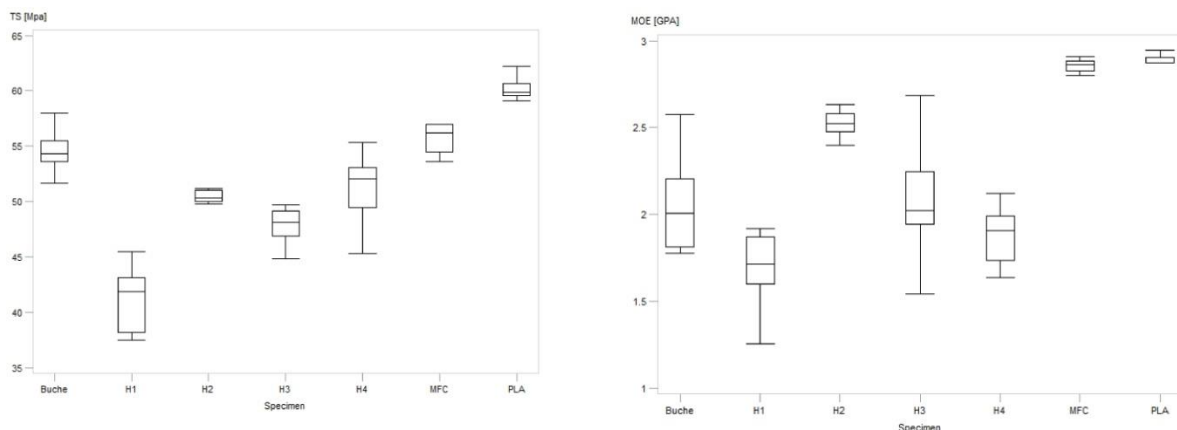


Figure 43 Tensile Test Composite Filament, left tensile strength, right Modulus of Elasticity

The statistical analysis of the tensile strength showed a significant variance. The model could explain 88% of the occurring variance. Tukey's test showed that neat PLA had a significant

difference to all other specimen. A slightly different statistical result showed the Modulus of Elasticity. The model describes 78% of the variance and Tukey's test showed that for neat PLA there was no significant distinction between MFC and H2 specimen.

4.6.2 Bending Test

Similar to the Tensile test in 4.6.1, Figure 44 shows that neat PLA, Buche and MFC had the best performance. There was no improvement of the mechanical properties with extra fibre load. Also the bending test showed, that the overall distribution of the fibres from Buche and MFC were better than that of the lignocellulosic samples. Buche showed the highest MOE with 3,37 [GPa], where neat PLA had the highest flexural strength with 139,03 [MPa] and the highest elongation at break with 20,16 [%]. Very obvious is the decreasing elongation at break with only 1 [%] fibre content, which is reduced by approx. 50 [%].

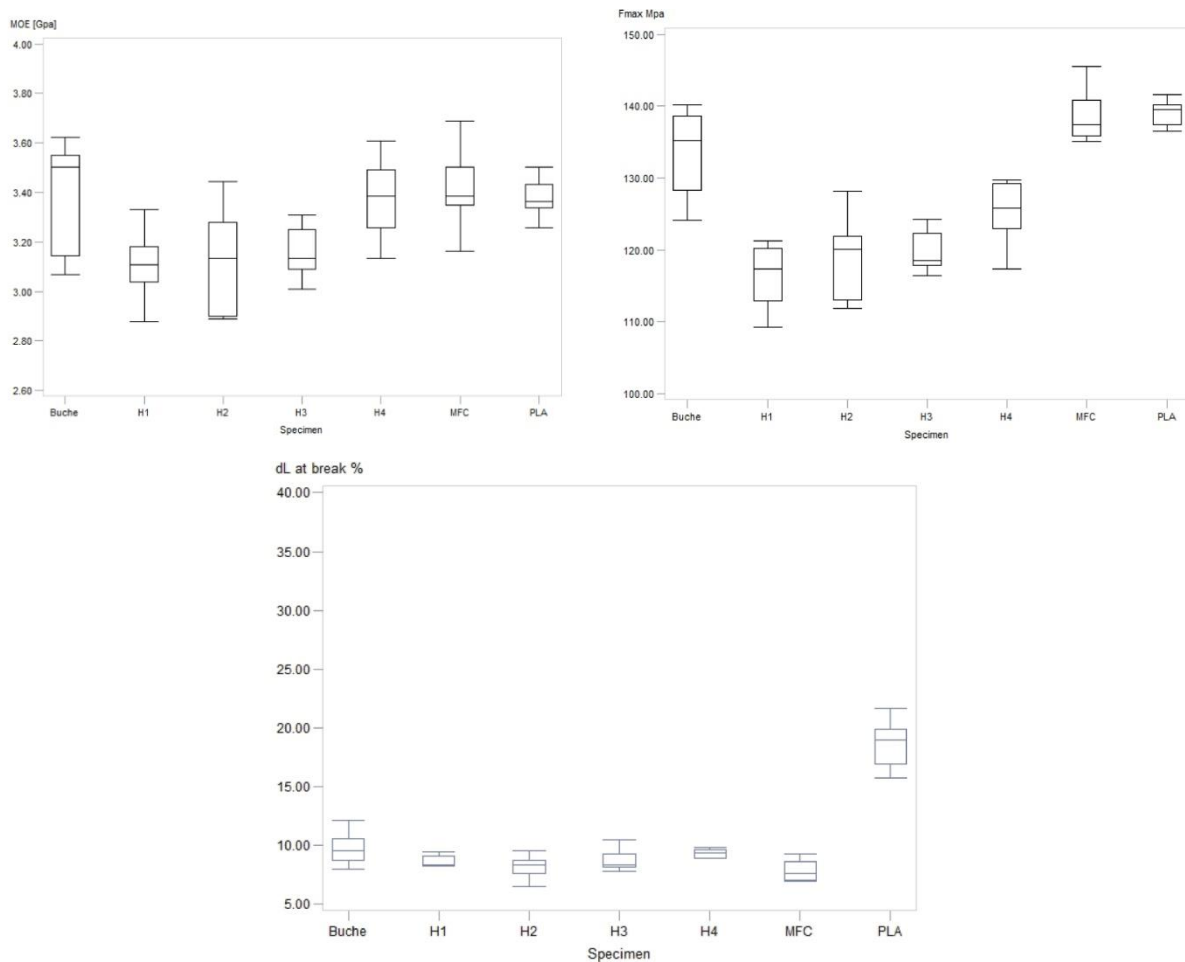


Figure 44 Left side Modulus of Elasticity, right side Flexural strength, below elongation at break

The statistical analyses for flexural strength showed a significant difference between the specimens. The Model explained 80 [%] of the data set. Tukey's test pointed out three different groups distinguishing as class (A) PLA, MFC and Buche. Second Class (B) with H3, H2 and H1 and class (C) with H4, which differs significantly from every other group. The ANOVA of the Modulus of elasticity showed a significant result but only with an R² of 33 [%].

4.6.3 Impact Test

The Charpy impact test indicated slightly increased impact strength of MFC, H4 and H3, with 0,976 [j/cm²], 1,05 [j/cm²] and 0,976 [j/cm²] compared to neat PLA, with a notched impact

strength of 0,878 [j/cm²]. The rest of the specimen had a slightly lower value and the statistical analysis showed no significant result with a p-value of 0.5. Therefore it can be presumed that the fibre load of 1[%] didn't influence the impact strength.

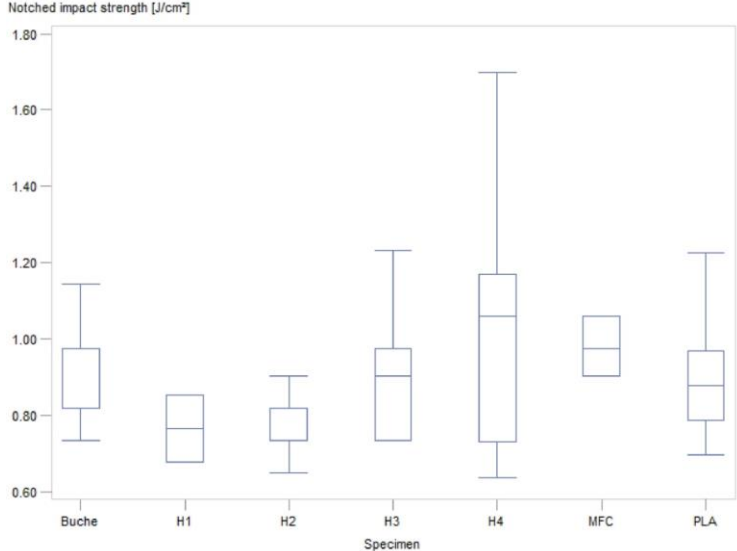


Figure 45 Impact test

4.6.4 MVR Test

The fibre load of 1% in the filament decreased the flow rate of the neat PLA as illustrated in Figure 46. The variety ranged from 14 [cm³/10min] (H4) to 20 [cm³/10min] (PLA), in which every composite containing a fibre load had a higher viscosity as the neat PLA. This fact can be interesting for further processing procedures such as injection moulding or fuse deposition modelling. Besides, a decrease of MVR can indicate a better fibre dispersion [26].

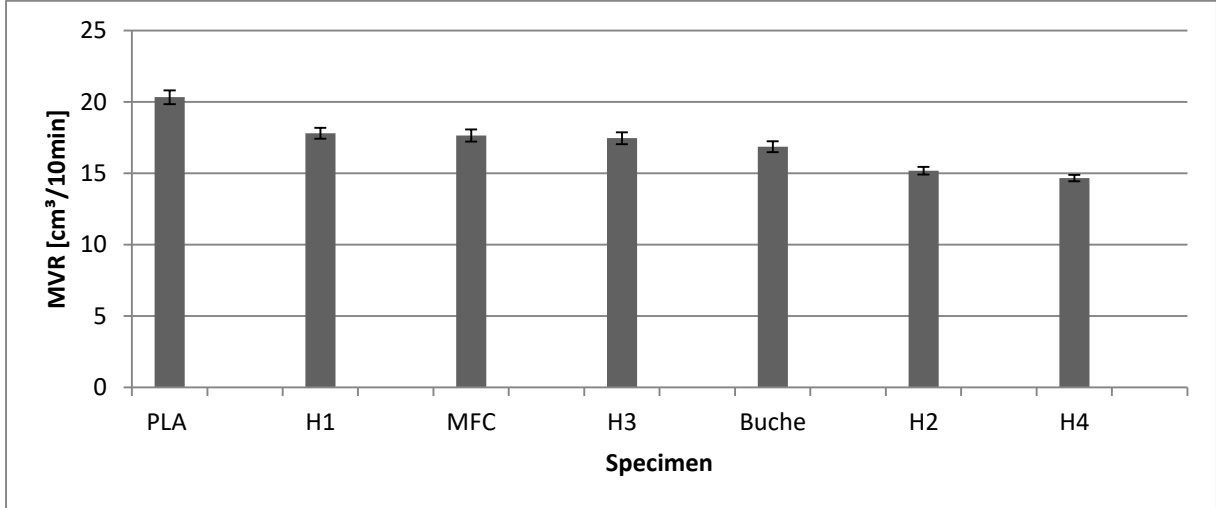


Figure 46 MVR test

4.6.5 Dynamic Mechanical Analyse composite filament (DMA)

The storage Modulus according to Figure 48, ranged from 4000 [MPa] for H2 to about 4800 [MPa] for neat PLA and the Buche Specimen. According to the mean value of the inflexion point of the storage modulus graph, the glass transition temperature of the different

specimen from 63,7 [°C] to 65,4 [°C]. The values of the averaged tan delta curve were slightly higher as shown in Figure 48. The peak temperature ranged from 69,6 [°C] for H4 to 71,9 [°C] for neat PLA specimen. The single values are given in Table 17 and Table 17.

Table 16 DMA composite filament, mean value inflexion points

Specimen filament	Temp at turning point Storage Modulus [°C]
H1	64,9
H2	65,1
H3	63,9
H4	63,7
MFC	64,9
Buche	64,9
PLA	65,4

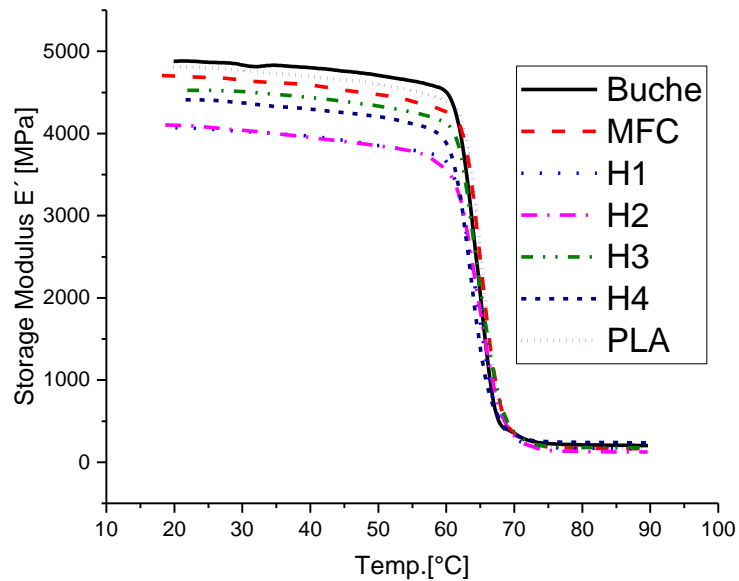


Figure 47 DMA characterization composite filament, average graphs storage Modulus E'

Table 17 DMA composite filament, mean values peaks tan delta

Specimen filament	Temp. at peak point from tan d [°C]
H1	71,1
H2	71,4
H3	71,4
H4	69,6
MFC	72,4
Buche	71,4
PLA	71,9

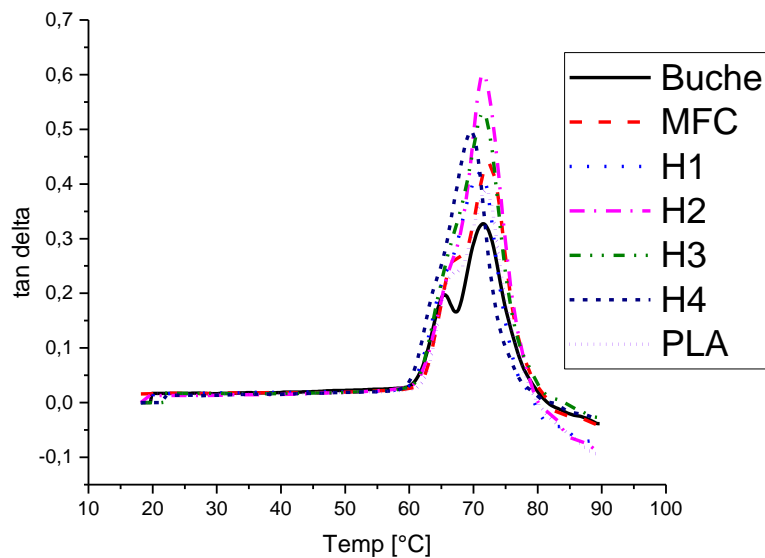
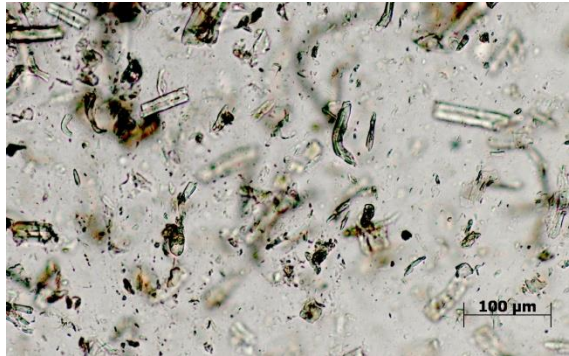


Figure 48 DMA characterization composite filament, average graphs t tan delta

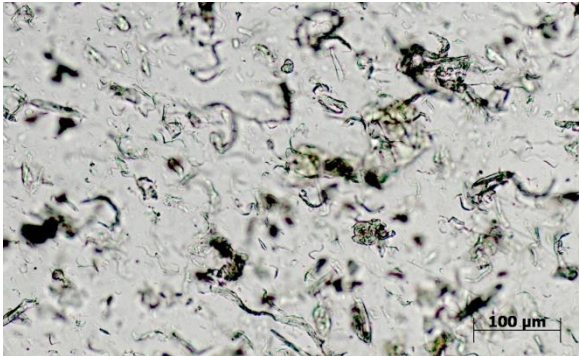
4.7 Qualitative Microscope characterisation

In order to investigate, if there is a different distribution in the specimens, they were cut in small slices and melted on the object carrier. Figure 49 shows the fibre distribution of the

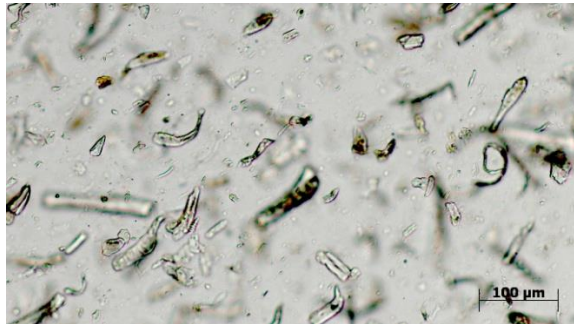
specimen H3, MFC, H4 and Buche. It turned out, that Buche and H4 had the bigger fibre type compared to MFC and H3. Especially Buche had very big fibre agglomerates. MFC seemed to have the smallest and better dispersed but also contains big agglomeration as in all other specimen. The qualitative characterisation of the fibre gave no conclusive reason why the compounded composites showed such a weak behaviour in comparison to the casted composite film.



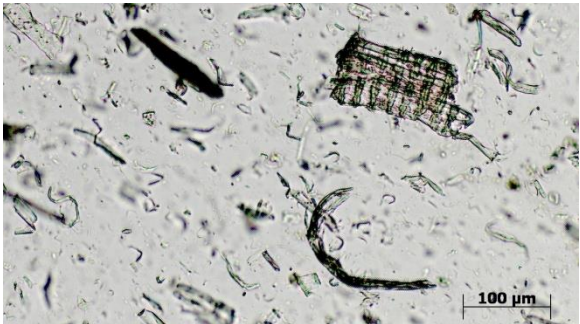
H3



MFC



H4



Buche

Figure 49 Fibre distribution in the filament composite specimen H3, MFC, H4 and Buche

5 Discussion

The use of MFLC (H1-H4) as a reinforcement material for polymer matrices, especially in the case of the casting process, showed a promising way to improve the mechanical properties. Nevertheless it revealed also several issues, which have to be addressed.

Comprehensively the following tables condense the mechanical properties of the crafted composites as well as their standard deviation. Table 18 shows the composite films with 1[%] fibre load, whereas Table 19 illustrates the composite filaments containing 1[%] fibre load.

Table 18 Averaged Values of mechanical properties test for composite films

Composite films [1%]	MOE [MPa]	STD (+/-)	σ_m [MPa]	STD (+/-)	Elongation at break [%]	STD (+/-)
PLA	902,5	60,06	27	0,83	13,86	3,68
Buche	871,67	47,92	25,29	1,09	11,17	1,95
H1	1153,13	99,31	32,19	1,89	5,54	0,69
H2	995,33	112,3	27,43	2,32	8,2	3,12
H3	1233,13	56,89	35,19	2,62	4,87	0,67
H4	1077,22	75,44	30,1	1,93	6,63	1,18
MFC	1075	138,5	29,37	4,09	5,76	0,86

Table 19 Averaged Values of mechanical properties test for composite filaments

Composite filament [1%]	MOE [MPa]	STD (+/-)	σ_m [MPa]	STD (+/-)	Elongation at break [%]	STD (+/-)
PLA	2889,3	43,91	60,23	1,12	3,08	0,13
Buche	2070,01	260,87	54,6	1,94	4,04	0,46
H1	1679,37	244,16	41,34	3,07	3,69	1,1
H2	2521,37	80,26	50,46	0,55	3,27	0,2
H3	2099,3	333,37	47,92	1,49	4,04	0,65
H4	1879,16	174,79	51,24	3,18	4,09	0,4
MFC	2855,81	41,77	55,73	1,37	3,05	0,07

Comparing these two tables, it is obvious that in general the extrusion process had the better performance according to material properties. In the casting process, neat PLA achieved a MOE of 902,5 [MPa] and a tensile strength of 27 [MPa] whereas in the extrusion process the PLA reached a MOE of 2889,3 [MPa] and a tensile strength of 60,23 [MPa].. The casted film only reached 55,17 [%] of the tensile strength according to the filament. Very interesting results were found in the specimen H3. In the casting process, H3 improved the neat PLA in terms of tensile strength by 37 [%]. The MOE increased by 28 [%], whereas the filament specimen was reduced by -20 [%] for TS and -27 [%] for MOE. According to the fibre characterization, it could be seen that the tensile strength of the MFLC specimens correlated with the adhesion force measurement of the AFM spectroscopy in chapter 4.1. Remarkably is the fact that this didn't correlate with the lignin content as expected.

Muensri et. al. showed that the reduction of Lignin had no impact on mechanical properties using coconut fibre in a gluten bio composite. In his survey he used bigger fibres with a diameter of 0,2-0,5 [mm] and reduced stepwise the lignin content from 40 to 20 %, which indeed is a huge amount comparing to the MFLC fibre used in the survey. There, the lignin

content ranged from 4 – 22 [%]. But this also indicates that the polar interaction is not the only relevant parameter for a better adhesion and hence, not exclusively responsible for improved mechanical properties [50].

Looking at the microscopy qualitative overview (chapter 4.3), it is evident, that the distribution in the MFLC composite films are better than in MFC and Buche fibres - especially in sample H3. Remarkable is the fact that in contrast to its good distribution in the composite film the miscibility in chapter 4.2 showed that the specimen H1, H2, and H4 were better dispersed than the sample H3. The sample H3 showed a strong precipitation in the solvent test, which didn't correlate qualitatively with the dispersion in the casted composite film.

In the casting process, it can be argued that the lignin on the cellulose improves the wetting of the fibre by the matrix and promoted the interaction abilities between fibre and matrix.

An additional theoretical explanation is given in Figure 50 inspired by Randriamahazaka (2015). It illustrates the behaviour of polymer brushes on surfaces according to the used solvent. The left and the middle brush shows two conformations in a good solvent, which indicates that the polarity is similar. With other words, they like each other. On the contrary the right brush illustrates, that a sort of buckling occurs in an unequal solvent. A disliking situation, in which the brush coil collapses.

PLA, as a hydrophobic compound, will enlarge their brushes in the solvent. This leads to an increased fibre/matrix networking in the mixed solution. During the drying phase, while the solvent is evaporating, the polymer brushes collapses and interlinks with the dispersed fibre. This result in a more stable network compared to the pure polymer and can be seen as mechanical adhesion improvement.

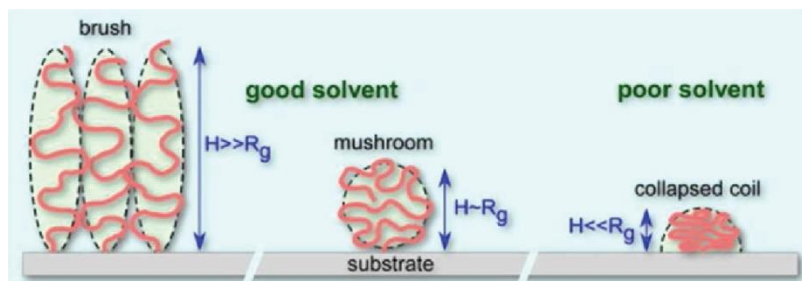


Figure 50 Schematic representation of polymer conformation anchored on surfaces, Source: [51]

Contrary to this observation, the DMA test drew a different picture. In the DMA measurement no changes for the TG temperature were detectable.

In a good fibre/matrix adhesion, it is expectable that in the transition zone a strong connection of matrix/fibre compound should lead to higher energy demand for leaving this state [26]. Compared to the other samples, the low tan delta peak of the neat PLA specimen indicated a poor adhesion between fibre and matrix. The ratio from loss modulus to storage modulus describes the tan delta peak ($E''/E' = \tan \delta$). It can be expected that in a good network, the storage modulus has a bigger influence and thus would lead to a reduced tan delta compared to the neat matrix material [49].

This also shows that, although the mechanical tests showed increasing properties, they are not enough to draw conclusions on the connectivity of fibre/matrix composites. Another theory could be that the used methods refer to different adhesion types. In a tensile test a very fixed and interlinked state is tested, which refers to a more mechanical adhesion interlink between fibre/matrix. The DMA measurement on the other hand describes an adhesion type which obviously occurs in a dynamical situation.

The distribution issue can also explain the test results of the filament composite. Through the mechanical treatment of the fibres, they had more fibrillated endings and these extra endings increased the agglomeration tendency in the dry state. This was also observed during the

extrusion process, in which the fibre clustered together in the hopper section. This cluster had to be removed manually, which lead to an unequal feeding of the fibres in the extrusion process. Because of these circumstances and in order to improve the dispersion of the fibres in the matrix, the compounding step was preformed twice. Apparently though, it had no effect to increase the dispersion rate in the compound. Maybe, in order to be beneficial, the compounding step would need to be repeated more than twice. But according to an oral communication to an polymer expert, additional compounding steps have the opposite effect and lead to a segregation [52].

Nevertheless, the agglomeration plus the additional high viscosity of the polymer melt in the extrusion screw, seems to block the dispersion of the fibres into the matrix material. Also the shearing forces of the screw didn't have any measurable mixing effect on them. Therefore tensile and bending tests showed decreasing properties and a DMA analysis didn't present changes in the composite films of the Tg value either.

Eyholzer et. al. explained with 1.Hexanol modified cellulose for extrusion, that the most challenging issue is the dispersion of the fibres in the matrix during this process [53]. Contrary Jonoobi et. al. extruded PLA with untreated cellulose nanofibres with an amount of 1[%], 3[%] and 5 [%]. In his studies he observed rising tensile strength as well as the MOE and Tg temperature in comparison to the neat PLA. But also his team pointed out that achieved distribution of their fibre is not sufficient [54].

The deterioration of the composite filament can be also explained by the last Figure 50. We can expect that in the extrusion process, small polymer brushes with a low surface area are the common species in the polymer melt and thus the fibre and polymer had fewer possibilities to interact with each other.

To overcome this problem, the Institute of renewable resources on the college in Magdeburg Stendal tried to extrude the PLA directly with an aqueous fibre bacterial nano cellulose solution. They used a modified extrusion screw with additional emerging water outlets. The researchers achieved a very diffuse picture with some increased and also decreased mechanical properties of their modified PLA. As well in their case they suspected clustering of the fibres and according to the agglomeration a bad dispersion in the matrix [55]. Remarkably about this survey is the fact that it seemed they had no problem with autocatalytic hydrolysatation of the PLA compound. Several degradation studies demonstrated that PLA decomposition rate is increased and influenced by the water content [56].

6 Conclusion

For a real breakthrough in sustainable composite development the biggest challenge in the future will be the improvement of the dispersion of the reinforcing fibre material. This survey focused on the compatibility, in form of even and equal charge distribution, of reinforcing material and matrix material. There is no doubt that the polarity is one factor which facilitates the distribution and adhesion, but there are different relevant parameters to address in order to achieve a better distribution in the matrix. Cellulosic fibres have the tendency to form hydrogen bonds with adjacent fibrils which results in agglomeration of the fibres and hence hinders a broad dispersion in the matrix material. The focus should be set more on the reduction of the entanglement of this agglomeration. There are tons of ideas and methods in the scientific world how to address this problem and to modify the surface of the fibres to reduce hydrogen bonding.

The advantage of MFLC fibres are, that the treatment method used to derive this sort of fibre is a cleaner, more sustainable way to extract them compared to standard technology. No further chemical modification is necessary, hence there is no need of toxic modification chemicals.

The dispersion in film casting can be easily improved. Different polymer/solution/fibre systems can be tested. A big advantage would be to get rid of the highly toxic chloroform solvent. Swelling, mixing and drying process during film casting can be modified with little effort.

Furthermore, the huge variety in the fibre resource base must be tested. Maybe softwood MFLC fibres treated in an organosolve process should be tried. It would be interesting to see, if extractives in the softwood MFLC pulp leads to a further step of surface modification during the process. Contrary to the fibre resource base, the matrix could be modified in the mean of acid-base adhesion theory. There are several end functionalized PLA components with different chemical functional groups. A main disadvantage could be the low molecular weight compared to neat PLA.

Another task is to determine the right adhesion models occurring in the developed composite systems. Which fits better and is it possible to model it with a computer based model? This would help to understand the needed pre-treatment for fibres or matrix material more detailed. As well it would determine a good starting point to handle the next big task. Film casting to determine the miscibility is a good and fast scientific method to determine if fibre/matrix system can be connected, but it cannot address the dispersion issue on an industrial scale.

Extrusion, injection moulding or fuse despositioning processes are the most common techniques in the industry and the survey showed that although an improvement in film casting can be seen, it doesn't mean that this also occurs in other processes. In these processes the high viscosity of the matrix material additionally increases the problem of miscibility. There is more work to be done, to enhance the diffusion of fibres into the bulk material. Maybe commercially available extrusion machines are not perfectly equipped for this task. More sophisticated machines could be able to use aqueous or even perfect matched solvent system in the extrusion process. But this also indicates to find non-toxic and environmental friendly solvent system.

Ultimately following questions should be worked out in order to achieve a sustainable way for using MFLC. What are additional benefits of merging MFCL into polymers? Referring to chapter 2.1.2, not only mechanical properties should be focused on. What are the humidity or air barrier properties, e.g. in packaging industries? Another aim can be to increase the lifespan of the material or its resistance to different solvent systems. Also the use of insulation material with improved thermal or electrical properties can be of interest.

But in every case mentioned above, a good dispersion from fibre in the matrix polymer is crucial, to achieve homogenous material properties. Therefore more research work has to be done.

7 Bibliography

- [1] Elsner Peter, Peter Eyerer, and Thomas Hirth, *Domininghaus - Kunststoffe*, 8th ed. Berlin-Heidelberg: Springer, 2012.
- [2] M. Eriksen *et al.*, 'Plastic Pollution in the World's Oceans: More than 5 Trillion Plastic Pieces Weighing over 250,000 Tons Afloat at Sea', *PLOS ONE*, vol. 9, no. 12, p. e111913, Dec. 2014.
- [3] S. Werner, 'Auswirkung von Meeresmüll'. Umweltbundesamt, 08-Apr-2013.
- [4] H. Schroeder, *Lehmbau - Mit Lehm ökologisch planen und bauen*, 2nd ed. Wiesbaden: Springer Fachmedien, 2013.
- [5] A. Winter *et al.*, 'Reduced polarity and improved dispersion of microfibrillated cellulose in poly(lactic-acid) provided by residual lignin and hemicellulose', *J. Mater. Sci.*, vol. 52, no. 1, pp. 60–72, 2017.
- [6] W. Gindl-Altmutter, M. Obersriebnig, S. Veigel, and F. Liebner, 'Compatibility between Cellulose and Hydrophobic Polymer Provided by Microfibrillated Lignocellulose', *ChemSusChem*, vol. 8, no. 1, pp. 87–91, 2015.
- [7] S. Herzele, 'Herstellung und Eigenschaften von mikrofibrillierter Lignocellulose als Verstärkungsfasern in ausgewählten Matrixpolymeren', Master Thesis, Universität Hamburg, Hamburg, 2014.
- [8] E. Witten, *Handbuch Faserverbundkunststoffe/Composites*, 4th ed. Frankfurt am Main: Springer Vieweg, 2013.
- [9] P. Srikanth, *Handbook of Bioplastics and Biocomposites Engineering Applications*. New Jersey, Hoboken: John Wiley & Sons, Inc., 2011.
- [10] 'Adhesion', *Dictionary.com*, 30-Nov-2016. [Online]. Available: [Dictionary.com http://www.dictionary.com/browse/adhesion](http://www.dictionary.com/browse/adhesion).
- [11] D. J. Gardner, M. Blumentritt, L. Wang, and N. Yildirim, 'Adhesion Theories in Wood Adhesive Bonding', in *Progress in Adhesion and Adhesives*, John Wiley & Sons, Inc., 2015, pp. 125–168.
- [12] H. Gleich, 'Zusammenhang zwischen Oberflächenenergie und Adhäsionsvermögen von Polymerwerkstoffen am Beispiel von PP und PBT und deren Beeinflussung durch die Niederdruck-Plasmatechnologie', Duisburg-Essen, Duisburg, 2004.
- [13] V. Dutschk, 'Oberflächenkräfte und ihr Beitrag zu Adhäsion und Haftung in glasfaserverstärkten Thermoplasten', Technische Universität Dresden, Dresden, 2000.
- [14] M. Nardin and J. Schultz, 'Relationship between fibre-matrix adhesion and the interfacial shear strength in polymer-based composites', *Science & Technology*, vol. 1, no. 2, 1993.
- [15] R. Gibson, *Principles of composite material mechanics*. New York: CRC Press, 2007.
- [16] A. Godara, D. Raabe, I. Bergmann, R. Putz, and U. Müller, 'Influence of additives on the global mechanical behavior and the microscopic strain localization in wood reinforced polypropylene composites during tensile deformation investigated using digital image correlation', *Compos. Sci. Technol.*, vol. 69, no. 2, pp. 139–146, Feb. 2009.
- [17] S. Migneault, A. Koubaa, F. Erchiqui, A. Chaala, K. Englund, and M. P. Wolcott, 'Application of micromechanical models to tensile properties of wood-plastic composites', *Wood Sci. Technol.*, vol. 45, no. 3, pp. 521–532, 2011.
- [18] T. T. Law, Y. J. Phua, R. Senawi, A. Hassan, and Z. A. Mohd Ishak, 'Experimental analysis and theoretical modeling of the mechanical behavior of short glass fiber and short carbon fiber reinforced polycarbonate hybrid composites', *Polym. Compos.*, vol. 37, no. 4, pp. 1238–1248, 2016.
- [19] S. Migneault, A. Koubaa, F. Erchiqui, A. Chaala, K. Englund, and M. P. Wolcott, 'Application of micromechanical models to tensile properties of wood-plastic composites', *Wood Sci. Technol.*, vol. 45, no. 3, pp. 521–532, 2011.

- [20]S. Deng, L. Ye, and Y.-W. Mai, 'Influence of fibre cross-sectional aspect ratio on mechanical properties of glass fibre/epoxy composites I. Tensile and flexure behaviour', *Compos. Sci. Technol.*, vol. 59, no. 9, pp. 1331–1339, Jul. 1999.
- [21]S. Chakraborty, *Mechanics over Micro and Nano Scales*, 1st ed. New York: Springer Verlag, 2011.
- [22]Hongzhang Chen, *Biotechnology of Lignocellulose*. Dordrecht: Springer, 2014.
- [23]A. Wagenführ and F. Schloz, *Taschenbuch der Holztechnik*, 2nd ed. Leipzig: Carl Hanser, 2012.
- [24]T. Zimmermann, 'Cellulose Fibrils in Wood cell walls and their potential for technical applications', Hamburg, Zürich, 2007.
- [25]M. R. Roger, *Wood chemistry and wood composites*. Tylor & Francis, 2005.
- [26]T. Zimmermann, E. Pöhler, and T. Geiger, 'Cellulose Fibrils for Polymer Reinforcement', *Advanced Engineering Materials*, vol. 6, no. 9, 2004.
- [27]J. Martinka, E. Hroncov, T. Chrebet, and B. Karol, 'The influence of spruce wood heat treatment on its thermal stability and burning process', *Eur. J. Wood Wood Prod.*, vol. 72, no. 4, pp. 477–486, 2014.
- [28]D. Fengel and G. Wegener, *Wood:Chemistry, ultrastructure, Reactions*. Berlin: Walter De Gruyter, 1989.
- [29]D.-Y. Kim, Y. Nishiyama, M. Wada, S. Kuga, and T. Okano, 'Thermal decomposition of cellulose crystallites in wood', *Holzforschung*, vol. 55, no. 5, pp. 521–524, 2001.
- [30]C. Hill, *Wood modification*. West Sussex: John Wiley & Sons Ltd, 2006.
- [31]J. Lunte, 'Large scale production, properties and commercial applications of polylactic acid polymers.', no. 59, pp. 52–145, 1998.
- [32]K. J. Jem, J. F. van der Pol, and S. de Vos, 'Microbial Lactic Acid, Its Polymer Poly(lactic acid), and Their Industrial Applications', in *Plastics from Bacteria: Natural Functions and Applications*, G. G.-Q. Chen, Ed. Berlin, Heidelberg: Springer Berlin Heidelberg, 2010, pp. 323–346.
- [33]F. A. Castillo Martinez, E. M. Balciunas, J. M. Salgado, J. M. Domínguez González, A. Converti, and R. P. de S. Oliveira, 'Lactic acid properties, applications and production: A review', *Trends Food Sci. Technol.*, vol. 30, no. 1, pp. 70–83, Mar. 2013.
- [34]O. Türk, *Stoffliche Nutzung nachwachsender Rohstoffe*. Heidelberg: Springer Vieweg, 2013.
- [35]D. Garlotta, 'A literature review of poly(lactic acid)', *J. Polym. Environ.*, vol. 9, no. 2, pp. 63–84, 2001.
- [36]P. Yucheng, J. G. Douglas, and H. Yousoo, 'Drying cellulose nanofibrils: in search of a suitable method', vol. 19, 2011.
- [37]S. Muders and Pittman, 'Lösungsmittel', *chemie.de*, 18-Mar-2016. [Online]. Available: <http://www.chemie.de/lexikon/L%C3%B6sungsmittel.html>. [Accessed: 20-Mar-2016].
- [38]'Büchner flask', *Wikipedia*. [Online]. Available: https://en.wikipedia.org/wiki/B%C3%BCchner_flask. [Accessed: 20-Mar-2016].
- [39]E. TURK, 'Phosgen from Chloroform', *Chem. Eng. News Arch.*, vol. 76, no. 9, p. 6, Mar. 1998.
- [40]D. C. Jiles, *Introduction to the Principles of Materials Evaluation*. Boca Raton: CRC Press Taylor& Francis group, 2007.
- [41]'Stress strain curve', *University of Texas*, 2016. [Online]. Available: <http://web.uta.edu/faculty/ricard/Courses/KINE-3301/Notes/Lesson-14.html>. [Accessed: 23-Nov-2016].
- [42]'Bending test', *Flexure Test*, 2016. [Online]. Available: <http://www.testresources.net/applications/by-test-type/flexural-test>. [Accessed: 23-Nov-2016].

- [43]Holzmann, Meyer, and Schumpich, *Technische Mechanik Festigkeitslehre*, 11th ed. Wiesbaden: Springer Vieweg, 2014.
- [44]Pyrometer, 'Biegemomenteverlauf', *Biegemomenteverlauf*, 2013. [Online]. Available: https://de.wikipedia.org/wiki/Biegemoment#/media/File:Biegemoment_Balken_Mittenlast.svg. [Accessed: 23-Nov-2016].
- [45]Krishnavedala, 'Stress distribution across beam', *Stress distribution across beam*, 2012. [Online]. Available: https://en.wikipedia.org/wiki/Flexural_strength#/media/File:Beam_stress.svg. [Accessed: 23-Nov-2016].
- [46]S. Kerry, 'Charpy Impact', *Fabbaloo*, 2014. [Online]. Available: <http://www.fabbaloo.com/blog/2014/6/15/design-of-the-week-diy-material-testing-machine>. [Accessed: 23-Nov-2016].
- [47]'MVR Messung', *Instron*. [Online]. Available: <http://www.instron.co.uk/en-gb/testing-solutions/by-test-type/rheology>
- [48]M. Bonnet, *Kunststofftechnik Grundlagen, Verarbeitung, Werkstoffauswahl und Fallbeispiele*, 2., Berarb. und erw. Aufl. Wiesbaden: Springer Vieweg, 2014.
- [49]M. S. Huda, A. K. Mohanty, L. T. Drzal, E. Schut, and M. Misra, "'Green" composites from recycled cellulose and poly(lactic acid): Physico-mechanical and morphological properties evaluation', *J. Mater. Sci.*, vol. 40, no. 16, pp. 4221–4229, 2005.
- [50]P. Muensri, T. Kunanopparat, P. Menut, and S. Siriwattanayotin, 'Effect of lignin removal on the properties of coconut coir fiber/wheat gluten biocomposite', *Compos. Part Appl. Sci. Manuf.*, vol. 42, no. 2, pp. 173–179, Feb. 2011.
- [51]H. Randriamahazaka and J. Ghilane, 'Electrografting and Controlled surface Functionalization of Carbon based Surfaces for Electroanalysis', *Electrochem. Commun.*, 2015.
- [52]R. Zirbs, 'Mündliche Mitteilung über: Separation des Füllermaterials durch mehrmaliges compoundieren mit einer Extruderschnecke', 15-Jun-2016.
- [53]C. Eyholzer, P. Tingaut, T. Zimmermann, and K. Oksman, 'Dispersion and Reinforcing Potential of Carboxymethylated Nanofibrillated Cellulose Powders Modified with 1-Hexanol in Extruded Poly(Lactic Acid) (PLA) Composites', *J. Polym. Environ.*, vol. 20, no. 4, pp. 1052–1062, 2012.
- [54]M. Jonoobi, J. Harun, A. P. Mathew, and K. Oksman, 'Mechanical properties of cellulose nanofiber (CNF) reinforced polylactic acid (PLA) prepared by twin screw extrusion', *Compos. Sci. Technol.*, vol. 70, no. 12, pp. 1742–1747, Oct. 2010.
- [55]P. Gerth, 'Optimierung der Materialeigenschaften von Biopolymeren durch Faserverstärkung mit biotechnologischen gewonnen Nanocellulose-Fasern"', KAT-Kompetenzzentrum Ingenieurwissenschaften/Nachwachsende Rohstoffe, Hochschule Magdeburg-Stendal, Magdeburg, Abschlussbericht AZ 28651-31, 2012.
- [56]G. L. Siparsky, K. J. Voorhees, and F. Miao, 'Hydrolysis of Polylactic Acid (PLA) and Polycaprolactone (PCL) in Aqueous Acetonitrile Solutions: Autocatalysis', *J. Environ. Polym. Degrad.*, vol. 6, no. 1, pp. 31–41, 1998.

8 Appendix A technical data sheet matrix material



Ingeo™ Biopolymer 4043D Technical Data Sheet

Biaxially Oriented Films – General Purpose

Film Characteristics/ Applications

Ingeo 4043D – a product from NatureWorks LLC – can be converted into a biaxially oriented film with use temperatures up to 265°F (130°C). This film has excellent optics, good machinability and excellent twist and deadfold. These properties make 4043D film an ideal candidate for candy twist wrap and other packaging applications. Additional properties include advantageous barrier to flavor and grease and superior oil resistance.

Polymer Characteristics

4043D polymer is available in pellet form. Drying prior to processing is essential. The polymer is stable in the molten state, provided that the extrusion and drying procedures are followed.

Machine Configuration

Ingeo polymers will process on conventional extruders using general purpose screws with L/D ratios from 24:1 to 30:1 and compression ratio of 2.5:1 to 3:1. Smooth barrels are recommended. Ingeo resins will process on conventional cast tenter equipment that has been designed for OPS or OPET with minimal modifications. Optimization to your specific equipment may require NatureWorks LLC technical support

Process Details

Startup and Shutdown

Ingeo 4043D is not compatible with a wide variety of polyolefin resins, and special purging sequences should be followed:

1. Clean extruder and bring temperatures to steady state with low-viscosity, general-purpose polystyrene or high MFR polypropylene.
2. Vacuum out hopper system to avoid contamination.
3. Introduce Ingeo polymer into the extruder at the operating conditions used in Step 1.
4. Once Ingeo polymer has purged, reduce barrel temperatures to desired set points.
5. At shutdown, purge machine with high-viscosity polystyrene or polypropylene.

Typical Material & Application Properties ^(1, 2, 3)

Film Properties	Ingeo 4043D	ASTM Method	
Density	1.24 g/cc	D1505	
Tensile Strength	MD 16 kpsi	D882	
	TD 21 kpsi	D882	
Tensile Modulus	MD 480 kpsi	D882	
	TD 560 kpsi	D882	
Elongation at Break	MD 160%	D882	
	TD 100%	D882	
Elmendorf Tear	MD 15 g/mil	D1922	
	TD 13 g/mil	D1922	
Spencer Impact	2.5 joules		
Transmission Rates	Oxygen	675 cc-mil/ m ² -24hr-atm	D1434
	Carbon Dioxide	2,850 cc-mil/ m ² -24hr-atm	Internal
	Water Vapor	375 g-mil/ m ² -24hr	F1249
Optical Characteristics	Haze	2.1%	D1003
	Gloss, 20°	90	D1003
Thermal Characteristics	Melting Point	145-160°C	D3418

(1) Typical properties; not to be construed as specifications.

(2) All properties measured on 1.0 mil film.

(3) Typical values for a film oriented 3.5x in MD and 5x in TD.

Processing Temperature Profile

Melt Temp.	410±15°F	210±8 °C
Feed Throat	113°F	45°C
Feed Temp.	355°F	180°C
Compression Section	375°F	190°C
Metering Section	390°F	200°C
Adapter	390°F	200°C
Die	390°F	200°C
Screw Speed	20-100 rpm	
MD Draw Temp.	140-160°F	60-70°C
TD Draw Temp.	160-175°F	70-80°C

Drying

In-line drying is required. A moisture content of less than 0.025% (250ppm) is recommended to prevent viscosity degradation. Typical drying conditions are 4 hours at 175°F (80°C) or to a dew point of -30°F (-35°C), with an airflow rate greater than 0.5 cfm/lb of resin throughput. The resin should not be exposed to atmospheric

9 Appendix B Composite film calculation

Casting composite Film				
Measurements				
diameter Petri Dish	9,00 [cm]	Mass density*Volume	=	0,83 g
wanted film thickness	0,01 [cm]	for 2 films		1,65 g
Density PLA	1,30 [g/cm ³]	Suspension PLA		0,05 w%

1 Step	Amount of 2 films with 1% fibre load		1 Step	Amount of 2 films with 10% fibre load	
	Fibre amount	0,02 g		Fibre amount	0,17 g
	PLA amount	1,64 g		PLA amount	1,49 g
2 Step	preparing bottle for casting process with excess PLA	2 g	PLA	preparing bottle for casting process with excess PLA	1,8 g
	Casting amount	40 g	Suspension with PLA	Casting amount	36 g
3 Step	Ratio 99% PLA to 1% fibre	0,01		Ratio 90% PLA to 10% fibre	0,11
	Mixing dried fibre load	0,0202 g	fibre	Mixing dried fibre load	0,2000 g
4 Step	Modification of the casting bottle suspension		4 Step	Modification of the casting bottle suspension	
	New suspension mass	2,02 g		New suspension mass	2,00 g
	Chloroform mass (evaporation during casting neglected)	37,98 g		Chloroform mass (evaporation during casting neglected)	34,00 g
	New weight percent	5,319 %		New weight percent	5,882 %
5 Step	weight out of the casting bottle on petri dish		5 Step	weight out of the casting bottle on petri dish	
	newmass = mass*new weight percent	15,548 g	Suspension	newmass = mass*new weight percent	14,059 g
	Filling quantity	11,960 ml		Filling quantity	10,815 ml

Versuchsart: Datum: 05.02.15 Basis Rezeptur: 7.6.6a Variante: 14

Normaleigenschaften:		Titian 58		CM 45		NCT 55	
Einstruder:	<input type="checkbox"/> Titan 58	<input type="checkbox"/> CM 45	<input type="checkbox"/> NCT 55				
Schwabe:	750.3	700	700	001			
Form:	Präfer	Granulat	Granulat	002			
	Präfer	Präfer	Präfer	003			
	Präfer	Präfer	Präfer	004			
Schüttgewicht:	g						
Porositätszahl:	%						
Temperatur:	Soll [°C]	Ist [°C]					
Korngr.:	720	720					
Zylinder T1:	720	720					
Zylinder T2:	720	720					
Zylinder T3:	720	720					
Zylinder T4:	720	720					
Werkzeug T1:	720	720					
Werkzeug T2:	720	720					
Werkzeug T3:	720	720					
Werkzeug T4:	720	720					
Werkzeug T5:	720	720					
Werkzeug T6:	720	720					
Werkzeug T7:	720	720					
Werkzeug T8:	720	720					
Einstruderparameter:							
Drehzahl [U/min]	63						
Polenanzahl [mm]	63						
Motorstrom [A]	5.9						
Motortemp. [°C]	78						
Beimung [N]	17.1						

Beimung: 2.2 Compensiere 1
Drehung Stellzahl 320

Versuchsart: Datum: 05.02.15 Basis Rezeptur: 7.6.6a Variante: 13

Normaleigenschaften:		Titian 58		CM 45		NCT 55	
Einstruder:	<input type="checkbox"/> Titan 58	<input type="checkbox"/> CM 45	<input type="checkbox"/> NCT 55				
Schwabe:	750.3	700	700	001			
Form:	Präfer	Granulat	Granulat	002			
	Präfer	Präfer	Präfer	003			
	Präfer	Präfer	Präfer	004			
Schüttgewicht:	g						
Porositätszahl:	%						
Temperatur:	Soll [°C]	Ist [°C]					
Korngr.:	720	720					
Zylinder T1:	720	720					
Zylinder T2:	720	720					
Zylinder T3:	720	720					
Zylinder T4:	720	720					
Werkzeug T1:	720	720					
Werkzeug T2:	720	720					
Werkzeug T3:	720	720					
Werkzeug T4:	720	720					
Werkzeug T5:	720	720					
Werkzeug T6:	720	720					
Werkzeug T7:	720	720					
Werkzeug T8:	720	720					
Einstruderparameter:							
Drehzahl [U/min]	63						
Polenanzahl [mm]	63						
Motorstrom [A]	5.9						
Motortemp. [°C]	78						
Beimung [N]	17.1						

Beimung: 2.2 Compensiert

Versuchsart: Datum: 05.02.15 Basis Rezeptur: 7.6.6a Variante: 12

Normaleigenschaften:		Titian 58		CM 45		NCT 55	
Einstruder:	<input type="checkbox"/> Titan 58	<input type="checkbox"/> CM 45	<input type="checkbox"/> NCT 55				
Schwabe:	750.3	700	700	001			
Form:	Präfer	Granulat	Granulat	002			
	Präfer	Präfer	Präfer	003			
	Präfer	Präfer	Präfer	004			
Schüttgewicht:	g						
Porositätszahl:	%						
Temperatur:	Soll [°C]	Ist [°C]					
Korngr.:	720	720					
Zylinder T1:	720	720					
Zylinder T2:	720	720					
Zylinder T3:	720	720					
Zylinder T4:	720	720					
Werkzeug T1:	720	720					
Werkzeug T2:	720	720					
Werkzeug T3:	720	720					
Werkzeug T4:	720	720					
Werkzeug T5:	720	720					
Werkzeug T6:	720	720					
Werkzeug T7:	720	720					
Werkzeug T8:	720	720					
Einstruderparameter:							
Drehzahl [U/min]	63						
Polenanzahl [mm]	63						
Motorstrom [A]	4.6						
Motortemp. [°C]	78						
Beimung [N]	17.1						

Beimung: 2.2 Compensiere
Vorführung durch Vorreinigung
in der Vorrichtung
= 2000 U/min
Grundrohr
= Drehzahl Normwert 290 kein 24
Granulat

Versuchsart: Datum: 05.02.15 Basis Rezeptur: 7.6.6a Variante: 11

Normaleigenschaften:		Titian 58		CM 45		NCT 55	
Einstruder:	<input type="checkbox"/> Titan 58	<input type="checkbox"/> CM 45	<input type="checkbox"/> NCT 55				
Schwabe:	750.3	700	700	001			
Form:	Präfer	Granulat	Granulat	002			
	Präfer	Präfer	Präfer	003			
	Präfer	Präfer	Präfer	004			
Schüttgewicht:	g						
Porositätszahl:	%						
Temperatur:	Soll [°C]	Ist [°C]					
Korngr.:	720	720					
Zylinder T1:	720	720					
Zylinder T2:	720	720					
Zylinder T3:	720	720					
Zylinder T4:	720	720					
Werkzeug T1:	720	720					
Werkzeug T2:	720	720					
Werkzeug T3:	720	720					
Werkzeug T4:	720	720					
Werkzeug T5:	720	720					
Werkzeug T6:	720	720					
Werkzeug T7:	720	720					
Werkzeug T8:	720	720					
Einstruderparameter:							
Drehzahl [U/min]	63						
Polenanzahl [mm]	63						
Motorstrom [A]	4.6						
Motortemp. [°C]	78						
Beimung [N]	17.1						

Beimung: 2.2 Compensiert
Vorführung durch Vorreinigung
in der Vorrichtung
= 2000 U/min
Grundrohr
= Drehzahl Normwert 290

10.2 Filament

Versuchs-Nr.: 11 Datum: 22.12.15 Basis Rezeptur: 11 Veraltete: 12

Rechnerisch Elementarteile: Form: Pulver <input checked="" type="checkbox"/> Granulat <input checked="" type="checkbox"/> Pellet <input checked="" type="checkbox"/> Metallpul <input checked="" type="checkbox"/> Schmelzpunkt: <input checked="" type="checkbox"/> g/l <input type="checkbox"/> Rohmaterial: <input checked="" type="checkbox"/>		Basiskonzepte: Titan 58 <input checked="" type="checkbox"/> CM 45 <input checked="" type="checkbox"/> NCT 05 <input checked="" type="checkbox"/> 750.3 <input checked="" type="checkbox"/> 300 <input checked="" type="checkbox"/> 001 <input checked="" type="checkbox"/> 750.4 <input checked="" type="checkbox"/> 700 <input checked="" type="checkbox"/> 002 <input checked="" type="checkbox"/> 750.10 <input checked="" type="checkbox"/> 003 <input checked="" type="checkbox"/> Collin <input checked="" type="checkbox"/> 004 <input checked="" type="checkbox"/>	
Profilstruktur: Trichterhalter <input checked="" type="checkbox"/> <input type="checkbox"/> ja <input type="checkbox"/> nein <input type="checkbox"/> Trichterhalter <input checked="" type="checkbox"/> <input type="checkbox"/> ja <input type="checkbox"/> nein <input type="checkbox"/> Vakuum TK <input checked="" type="checkbox"/> <input type="checkbox"/> ja <input type="checkbox"/> nein <input type="checkbox"/> Kühlwanne <input checked="" type="checkbox"/> <input type="checkbox"/> ja <input type="checkbox"/> nein <input type="checkbox"/> Abzug <input checked="" type="checkbox"/> <input type="checkbox"/> ja <input type="checkbox"/> nein <input type="checkbox"/> Abst. Düse-Kalber <input checked="" type="checkbox"/> <input type="checkbox"/> ja <input type="checkbox"/> nein <input type="checkbox"/>		Einbauparameter: Drehzahl U/min: <u>37</u> Drehmoment Nm: <u>20</u> Messstrom I: <u>21</u> Messspannung U: <u>3,5</u> Belastung %: <u>100</u>	
Werkzeug: WK 11 <input checked="" type="checkbox"/> GK 3245 <input checked="" type="checkbox"/> WK 12 <input checked="" type="checkbox"/> GK 1648 <input checked="" type="checkbox"/> WK 13 <input checked="" type="checkbox"/> GK 021 <input checked="" type="checkbox"/> WK 14 <input checked="" type="checkbox"/> Eon ELG40 <input checked="" type="checkbox"/> WK 15 <input checked="" type="checkbox"/> FR 3 - kurz <input checked="" type="checkbox"/> WK 16 <input checked="" type="checkbox"/> FR 3 - lang <input checked="" type="checkbox"/> WK 17 <input checked="" type="checkbox"/> FR 4 - kurz <input checked="" type="checkbox"/> WK 18 <input checked="" type="checkbox"/> FR 4 - lang <input checked="" type="checkbox"/> WK 19 <input checked="" type="checkbox"/> FR 5.5 - kurz <input checked="" type="checkbox"/> WK 20 <input checked="" type="checkbox"/> FR 5.5 - lang <input checked="" type="checkbox"/> WK 21 <input checked="" type="checkbox"/> FR 6 - LPM <input checked="" type="checkbox"/> WK 22 <input checked="" type="checkbox"/> Sinterkiste <input checked="" type="checkbox"/> WK 23 <input checked="" type="checkbox"/> Platte 100x80 <input checked="" type="checkbox"/> WK 24 <input checked="" type="checkbox"/> Infrarotstrahlung <input checked="" type="checkbox"/> WK 25 <input checked="" type="checkbox"/> Profprofil 10x <input checked="" type="checkbox"/> WK 26 <input checked="" type="checkbox"/> Spritzplatte <input checked="" type="checkbox"/>		Granulstruktur: GK Frequenz <input checked="" type="checkbox"/> GK <input checked="" type="checkbox"/> Schöpfgeschicht <input checked="" type="checkbox"/> Granulfröhen <input checked="" type="checkbox"/> Durchsatz <input checked="" type="checkbox"/>	
Bemerkung: 36.1.15			

Versuchs-Nr.: 12 Datum: 22.12.15 Basis Rezeptur: 11 Veraltete: 13

Rechnerisch Elementarteile: Form: Pulver <input checked="" type="checkbox"/> Granulat <input checked="" type="checkbox"/> Pellet <input checked="" type="checkbox"/> Metallpul <input checked="" type="checkbox"/> Schmelzpunkt: <input checked="" type="checkbox"/> g/l <input type="checkbox"/> Rohmaterial: <input checked="" type="checkbox"/>		Basiskonzepte: Titan 58 <input checked="" type="checkbox"/> CM 45 <input checked="" type="checkbox"/> NCT 05 <input checked="" type="checkbox"/> 750.3 <input checked="" type="checkbox"/> 300 <input checked="" type="checkbox"/> 001 <input checked="" type="checkbox"/> 750.4 <input checked="" type="checkbox"/> 700 <input checked="" type="checkbox"/> 002 <input checked="" type="checkbox"/> 750.10 <input checked="" type="checkbox"/> 003 <input checked="" type="checkbox"/> Collin <input checked="" type="checkbox"/> 004 <input checked="" type="checkbox"/>	
Profilstruktur: Trichterhalter <input checked="" type="checkbox"/> <input type="checkbox"/> ja <input type="checkbox"/> nein <input type="checkbox"/> Trichterhalter <input checked="" type="checkbox"/> <input type="checkbox"/> ja <input type="checkbox"/> nein <input type="checkbox"/> Vakuum TK <input checked="" type="checkbox"/> <input type="checkbox"/> ja <input type="checkbox"/> nein <input type="checkbox"/> Kühlwanne <input checked="" type="checkbox"/> <input type="checkbox"/> ja <input type="checkbox"/> nein <input type="checkbox"/> Abzug <input checked="" type="checkbox"/> <input type="checkbox"/> ja <input type="checkbox"/> nein <input type="checkbox"/> Abst. Düse-Kalber <input checked="" type="checkbox"/> <input type="checkbox"/> ja <input type="checkbox"/> nein <input type="checkbox"/>		Einbauparameter: Drehzahl U/min: <u>32</u> Drehmoment Nm: <u>30</u> Messstrom I: <u>25,9</u> Messspannung U: <u>4,3</u> Belastung %: <u>100</u>	
Werkzeug: WK 11 <input checked="" type="checkbox"/> GK 3245 <input checked="" type="checkbox"/> WK 12 <input checked="" type="checkbox"/> GK 1648 <input checked="" type="checkbox"/> WK 13 <input checked="" type="checkbox"/> GK 021 <input checked="" type="checkbox"/> WK 14 <input checked="" type="checkbox"/> Eon ELG40 <input checked="" type="checkbox"/> WK 15 <input checked="" type="checkbox"/> FR 3 - kurz <input checked="" type="checkbox"/> WK 16 <input checked="" type="checkbox"/> FR 3 - lang <input checked="" type="checkbox"/> WK 17 <input checked="" type="checkbox"/> FR 4 - kurz <input checked="" type="checkbox"/> WK 18 <input checked="" type="checkbox"/> FR 4 - lang <input checked="" type="checkbox"/> WK 19 <input checked="" type="checkbox"/> FR 5.5 - kurz <input checked="" type="checkbox"/> WK 20 <input checked="" type="checkbox"/> FR 5.5 - lang <input checked="" type="checkbox"/> WK 21 <input checked="" type="checkbox"/> FR 6 - LPM <input checked="" type="checkbox"/> WK 22 <input checked="" type="checkbox"/> Sinterkiste <input checked="" type="checkbox"/> WK 23 <input checked="" type="checkbox"/> Platte 100x80 <input checked="" type="checkbox"/> WK 24 <input checked="" type="checkbox"/> Infrarotstrahlung <input checked="" type="checkbox"/> WK 25 <input checked="" type="checkbox"/> Profprofil 10x <input checked="" type="checkbox"/> WK 26 <input checked="" type="checkbox"/> Spritzplatte <input checked="" type="checkbox"/>		Granulstruktur: GK Frequenz <input checked="" type="checkbox"/> GK <input checked="" type="checkbox"/> Schöpfgeschicht <input checked="" type="checkbox"/> Granulfröhen <input checked="" type="checkbox"/> Durchsatz <input checked="" type="checkbox"/>	
Bemerkung: * am Schluss Polierung auf 200 V geschalt.			

Versuchs-Nr.: 13 Datum: 22.12.15 Basis Rezeptur: 11 Veraltete: 14

Rechnerisch Elementarteile: Form: Pulver <input checked="" type="checkbox"/> Granulat <input checked="" type="checkbox"/> Pellet <input checked="" type="checkbox"/> Metallpul <input checked="" type="checkbox"/> Schmelzpunkt: <input checked="" type="checkbox"/> g/l <input type="checkbox"/> Rohmaterial: <input checked="" type="checkbox"/>		Basiskonzepte: Titan 58 <input checked="" type="checkbox"/> CM 45 <input checked="" type="checkbox"/> NCT 05 <input checked="" type="checkbox"/> 750.3 <input checked="" type="checkbox"/> 300 <input checked="" type="checkbox"/> 001 <input checked="" type="checkbox"/> 750.4 <input checked="" type="checkbox"/> 700 <input checked="" type="checkbox"/> 002 <input checked="" type="checkbox"/> 750.10 <input checked="" type="checkbox"/> 003 <input checked="" type="checkbox"/> Collin <input checked="" type="checkbox"/> 004 <input checked="" type="checkbox"/>	
Profilstruktur: Trichterhalter <input checked="" type="checkbox"/> <input type="checkbox"/> ja <input type="checkbox"/> nein <input type="checkbox"/> Trichterhalter <input checked="" type="checkbox"/> <input type="checkbox"/> ja <input type="checkbox"/> nein <input type="checkbox"/> Vakuum TK <input checked="" type="checkbox"/> <input type="checkbox"/> ja <input type="checkbox"/> nein <input type="checkbox"/> Kühlwanne <input checked="" type="checkbox"/> <input type="checkbox"/> ja <input type="checkbox"/> nein <input type="checkbox"/> Abzug <input checked="" type="checkbox"/> <input type="checkbox"/> ja <input type="checkbox"/> nein <input type="checkbox"/> Abst. Düse-Kalber <input checked="" type="checkbox"/> <input type="checkbox"/> ja <input type="checkbox"/> nein <input type="checkbox"/>		Einbauparameter: Drehzahl U/min: <u>37</u> Drehmoment Nm: <u>20</u> Messstrom I: <u>21</u> Messspannung U: <u>3,5</u> Belastung %: <u>100</u>	
Werkzeug: WK 11 <input checked="" type="checkbox"/> GK 3245 <input checked="" type="checkbox"/> WK 12 <input checked="" type="checkbox"/> GK 1648 <input checked="" type="checkbox"/> WK 13 <input checked="" type="checkbox"/> GK 021 <input checked="" type="checkbox"/> WK 14 <input checked="" type="checkbox"/> Eon ELG40 <input checked="" type="checkbox"/> WK 15 <input checked="" type="checkbox"/> FR 3 - kurz <input checked="" type="checkbox"/> WK 16 <input checked="" type="checkbox"/> FR 3 - lang <input checked="" type="checkbox"/> WK 17 <input checked="" type="checkbox"/> FR 4 - kurz <input checked="" type="checkbox"/> WK 18 <input checked="" type="checkbox"/> FR 4 - lang <input checked="" type="checkbox"/> WK 19 <input checked="" type="checkbox"/> FR 5.5 - kurz <input checked="" type="checkbox"/> WK 20 <input checked="" type="checkbox"/> FR 5.5 - lang <input checked="" type="checkbox"/> WK 21 <input checked="" type="checkbox"/> FR 6 - LPM <input checked="" type="checkbox"/> WK 22 <input checked="" type="checkbox"/> Sinterkiste <input checked="" type="checkbox"/> WK 23 <input checked="" type="checkbox"/> Platte 100x80 <input checked="" type="checkbox"/> WK 24 <input checked="" type="checkbox"/> Infrarotstrahlung <input checked="" type="checkbox"/> WK 25 <input checked="" type="checkbox"/> Profprofil 10x <input checked="" type="checkbox"/> WK 26 <input checked="" type="checkbox"/> Spritzplatte <input checked="" type="checkbox"/>		Granulstruktur: GK Frequenz <input checked="" type="checkbox"/> GK <input checked="" type="checkbox"/> Schöpfgeschicht <input checked="" type="checkbox"/> Granulfröhen <input checked="" type="checkbox"/> Durchsatz <input checked="" type="checkbox"/>	
Bemerkung: 2.3.15			

Versuchs-Nr.: 14 Datum: 22.12.15 Basis Rezeptur: 11 Veraltete: 15

Rechnerisch Elementarteile: Form: Pulver <input checked="" type="checkbox"/> Granulat <input checked="" type="checkbox"/> Pellet <input checked="" type="checkbox"/> Metallpul <input checked="" type="checkbox"/> Schmelzpunkt: <input checked="" type="checkbox"/> g/l <input type="checkbox"/> Rohmaterial: <input checked="" type="checkbox"/>		Basiskonzepte: Titan 58 <input checked="" type="checkbox"/> CM 45 <input checked="" type="checkbox"/> NCT 05 <input checked="" type="checkbox"/> 750.3 <input checked="" type="checkbox"/> 300 <input checked="" type="checkbox"/> 001 <input checked="" type="checkbox"/> 750.4 <input checked="" type="checkbox"/> 700 <input checked="" type="checkbox"/> 002 <input checked="" type="checkbox"/> 750.10 <input checked="" type="checkbox"/> 003 <input checked="" type="checkbox"/> Collin <input checked="" type="checkbox"/> 004 <input checked="" type="checkbox"/>	
Profilstruktur: Trichterhalter <input checked="" type="checkbox"/> <input type="checkbox"/> ja <input type="checkbox"/> nein <input type="checkbox"/> Trichterhalter <input checked="" type="checkbox"/> <input type="checkbox"/> ja <input type="checkbox"/> nein <input type="checkbox"/> Vakuum TK <input checked="" type="checkbox"/> <input type="checkbox"/> ja <input type="checkbox"/> nein <input type="checkbox"/> Kühlwanne <input checked="" type="checkbox"/> <input type="checkbox"/> ja <input type="checkbox"/> nein <input type="checkbox"/> Abzug <input checked="" type="checkbox"/> <input type="checkbox"/> ja <input type="checkbox"/> nein <input type="checkbox"/> Abst. Düse-Kalber <input checked="" type="checkbox"/> <input type="checkbox"/> ja <input type="checkbox"/> nein <input type="checkbox"/>		Einbauparameter: Drehzahl U/min: <u>32</u> Drehmoment Nm: <u>30</u> Messstrom I: <u>25,9</u> Messspannung U: <u>4,3</u> Belastung %: <u>100</u>	
Werkzeug: WK 11 <input checked="" type="checkbox"/> GK 3245 <input checked="" type="checkbox"/> WK 12 <input checked="" type="checkbox"/> GK 1648 <input checked="" type="checkbox"/> WK 13 <input checked="" type="checkbox"/> GK 021 <input checked="" type="checkbox"/> WK 14 <input checked="" type="checkbox"/> Eon ELG40 <input checked="" type="checkbox"/> WK 15 <input checked="" type="checkbox"/> FR 3 - kurz <input checked="" type="checkbox"/> WK 16 <input checked="" type="checkbox"/> FR 3 - lang <input checked="" type="checkbox"/> WK 17 <input checked="" type="checkbox"/> FR 4 - kurz <input checked="" type="checkbox"/> WK 18 <input checked="" type="checkbox"/> FR 4 - lang <input checked="" type="checkbox"/> WK 19 <input checked="" type="checkbox"/> FR 5.5 - kurz <input checked="" type="checkbox"/> WK 20 <input checked="" type="checkbox"/> FR 5.5 - lang <input checked="" type="checkbox"/> WK 21 <input checked="" type="checkbox"/> FR 6 - LPM <input checked="" type="checkbox"/> WK 22 <input checked="" type="checkbox"/> Sinterkiste <input checked="" type="checkbox"/> WK 23 <input checked="" type="checkbox"/> Platte 100x80 <input checked="" type="checkbox"/> WK 24 <input checked="" type="checkbox"/> Infrarotstrahlung <input checked="" type="checkbox"/> WK 25 <input checked="" type="checkbox"/> Profprofil 10x <input checked="" type="checkbox"/> WK 26 <input checked="" type="checkbox"/> Spritzplatte <input checked="" type="checkbox"/>		Granulstruktur: GK Frequenz <input checked="" type="checkbox"/> GK <input checked="" type="checkbox"/> Schöpfgeschicht <input checked="" type="checkbox"/> Granulfröhen <input checked="" type="checkbox"/> Durchsatz <input checked="" type="checkbox"/>	
Bemerkung: 2.3.15			

Versuchsnr.: Datum: 21.11.15 Variante: H4 Basis Rezeptur: 11

Reinmaterial Eigenschaften: Form:	<input type="checkbox"/> Pulver <input checked="" type="checkbox"/> Granulat <input type="checkbox"/> Pellet <input type="checkbox"/> Metallpulver	<input checked="" type="checkbox"/> grobster <input checked="" type="checkbox"/> 100 µm <input type="checkbox"/> 200 µm <input type="checkbox"/> 400 µm <input type="checkbox"/> 600 µm <input type="checkbox"/> 800 µm <input type="checkbox"/> 1000 µm	<input checked="" type="checkbox"/> NCT 05 <input type="checkbox"/> 001 <input type="checkbox"/> 002 <input type="checkbox"/> 003 <input type="checkbox"/> 004
Schmelzgewicht: Pulverfeuchte:	g / %	<input type="checkbox"/> Vakuumier <input type="checkbox"/> offen <input checked="" type="checkbox"/> Material aus Engpassung:	<input type="checkbox"/> ja <input type="checkbox"/> nein
Temperatur: Soll [°C] Ist [°C]		<input checked="" type="checkbox"/> wasserdampfen <input type="checkbox"/> Dampf <input type="checkbox"/> Einleitvorrichtung <input type="checkbox"/> Doppeltvorrichtung	
Zylinder T1	170		
Zylinder T2	170		
Zylinder T3	170		
Zylinder T4	170		
Adapter			
Werkzeug T1	160		
Werkzeug T2			
Werkzeug T3			
Werkzeug T4			
Werkzeug T5			
Werkzeug T6			
Werkzeug T7			
Werkzeug T8			
Extrudierparameter: Durchsatz [L/h] 32 Rückdruck [bar] Mischzeit [s] 34 Mischzeit [°C] 157 Belastung [N/A] 20/1			

Druckung: grobster 100 µm 200 µm 400 µm 600 µm 800 µm 1000 µm

Profilfunktion: Trockenkühler Vakuumier Material aus Engpassung: ja nein

Granulierung: GK Frequenz GK CEI Ecom ELG400 FR 3 - kurz FR 3 - lang FR 4 - kurz FR 4 - lang FR 5.5 - kurz FR 5.5 - lang FR 6 - UPM Sesselschiebe Plato 10005 Bineozeltopf Proprüf 104 Strengplatte

Bemerkung: *Ein Loch zu klein → 2,07 L*
(ändert sich wieder, wenn Luft die Extruder

Versuchsnr.: Datum: 21.11.15 Variante: H4 Basis Rezeptur: 11

Reinmaterial Eigenschaften: Form:	<input type="checkbox"/> Pulver <input checked="" type="checkbox"/> Granulat <input type="checkbox"/> Pellet <input type="checkbox"/> Metallpulver	<input checked="" type="checkbox"/> grobster <input checked="" type="checkbox"/> 100 µm <input type="checkbox"/> 200 µm <input type="checkbox"/> 400 µm <input type="checkbox"/> 600 µm <input type="checkbox"/> 800 µm <input type="checkbox"/> 1000 µm	<input checked="" type="checkbox"/> NCT 05 <input type="checkbox"/> 001 <input type="checkbox"/> 002 <input type="checkbox"/> 003 <input type="checkbox"/> 004
Schmelzgewicht: Pulverfeuchte:	g / %	<input type="checkbox"/> Vakuumier <input type="checkbox"/> offen <input checked="" type="checkbox"/> Material aus Engpassung:	<input type="checkbox"/> ja <input type="checkbox"/> nein
Temperatur: Soll [°C] Ist [°C]		<input checked="" type="checkbox"/> wasserdampfen <input type="checkbox"/> Dampf <input type="checkbox"/> Einleitvorrichtung <input type="checkbox"/> Doppeltvorrichtung	
Zylinder T1	170		
Zylinder T2	170		
Zylinder T3	170		
Zylinder T4	170		
Adapter			
Werkzeug T1	160		
Werkzeug T2			
Werkzeug T3			
Werkzeug T4			
Werkzeug T5			
Werkzeug T6			
Werkzeug T7			
Werkzeug T8			
Extrudierparameter: Durchsatz [L/h] 32 Rückdruck [bar] Mischzeit [s] 33 Mischzeit [°C] 157 Belastung [N/A] 20/1			

Druckung: grobster 100 µm 200 µm 400 µm 600 µm 800 µm 1000 µm

Profilfunktion: Trockenkühler Vakuumier Material aus Engpassung: ja nein

Granulierung: GK Frequenz GK CEI Ecom ELG400 FR 3 - kurz FR 3 - lang FR 4 - kurz FR 4 - lang FR 5.5 - kurz FR 5.5 - lang FR 6 - UPM Sesselschiebe Plato 10005 Bineozeltopf Proprüf 104 Strengplatte

Bemerkung: *Zu Schuss, schlechte Verwindung
→ +5°C in 170
+Verwindung auf 200 erhöht
• Normwert melkt die Folie*

Versuchsnr.: Datum: 21.11.15 Variante: CM7 Basis Rezeptur: 11

Reinmaterial Eigenschaften: Form:	<input type="checkbox"/> Pulver <input checked="" type="checkbox"/> Granulat <input type="checkbox"/> Pellet <input type="checkbox"/> Metallpulver	<input checked="" type="checkbox"/> grobster <input checked="" type="checkbox"/> 100 µm <input type="checkbox"/> 200 µm <input type="checkbox"/> 400 µm <input type="checkbox"/> 600 µm <input type="checkbox"/> 800 µm <input type="checkbox"/> 1000 µm	<input checked="" type="checkbox"/> NCT 05 <input type="checkbox"/> 001 <input type="checkbox"/> 002 <input type="checkbox"/> 003 <input type="checkbox"/> 004
Schmelzgewicht: Pulverfeuchte:	g / %	<input type="checkbox"/> Vakuumier <input type="checkbox"/> offen <input checked="" type="checkbox"/> Material aus Engpassung:	<input type="checkbox"/> ja <input type="checkbox"/> nein
Temperatur: Soll [°C] Ist [°C]		<input checked="" type="checkbox"/> wasserdampfen <input type="checkbox"/> Dampf <input type="checkbox"/> Einleitvorrichtung <input type="checkbox"/> Doppeltvorrichtung	
Zylinder T1	170		
Zylinder T2	170		
Zylinder T3	170		
Zylinder T4	170		
Adapter			
Werkzeug T1	160		
Werkzeug T2			
Werkzeug T3			
Werkzeug T4			
Werkzeug T5			
Werkzeug T6			
Werkzeug T7			
Werkzeug T8			
Extrudierparameter: Durchsatz [L/h] 35 Rückdruck [bar] Mischzeit [s] 35 Mischzeit [°C] 157 Belastung [N/A] 20/1			

Druckung: grobster 100 µm 200 µm 400 µm 600 µm 800 µm 1000 µm

Profilfunktion: Trockenkühler Vakuumier Material aus Engpassung: ja nein

Granulierung: GK Frequenz GK CEI Ecom ELG400 FR 3 - kurz FR 3 - lang FR 4 - kurz FR 4 - lang FR 5.5 - kurz FR 5.5 - lang FR 6 - UPM Sesselschiebe Plato 10005 Bineozeltopf Proprüf 104 Strengplatte

Bemerkung: *Anlage Verwindung der Zylinder
bei 200 UPM Verwindung
• Zu Schuss, vermindert
• schlechte Hydratation im
Fluss*

Versuchsnr.: Datum: 22.11.15 Variante: H4 Basis Rezeptur: 11

Reinmaterial Eigenschaften: Form:	<input type="checkbox"/> Pulver <input checked="" type="checkbox"/> Granulat <input type="checkbox"/> Pellet <input type="checkbox"/> Metallpulver	<input checked="" type="checkbox"/> grobster <input checked="" type="checkbox"/> 100 µm <input type="checkbox"/> 200 µm <input type="checkbox"/> 400 µm <input type="checkbox"/> 600 µm <input type="checkbox"/> 800 µm <input type="checkbox"/> 1000 µm	<input checked="" type="checkbox"/> NCT 05 <input type="checkbox"/> 001 <input type="checkbox"/> 002 <input type="checkbox"/> 003 <input type="checkbox"/> 004
Schmelzgewicht: Pulverfeuchte:	g / %	<input type="checkbox"/> Vakuumier <input type="checkbox"/> offen <input checked="" type="checkbox"/> Material aus Engpassung:	<input type="checkbox"/> ja <input type="checkbox"/> nein
Temperatur: Soll [°C] Ist [°C]		<input checked="" type="checkbox"/> wasserdampfen <input type="checkbox"/> Dampf <input type="checkbox"/> Einleitvorrichtung <input type="checkbox"/> Doppeltvorrichtung	
Zylinder T1	170		
Zylinder T2	170		
Zylinder T3	170		
Zylinder T4	170		
Adapter			
Werkzeug T1	160		
Werkzeug T2			
Werkzeug T3			
Werkzeug T4			
Werkzeug T5			
Werkzeug T6			
Werkzeug T7			
Werkzeug T8			
Extrudierparameter: Durchsatz [L/h] 32 Rückdruck [bar] Mischzeit [s] 33 Mischzeit [°C] 157 Belastung [N/A] 20/1			

Druckung: grobster 100 µm 200 µm 400 µm 600 µm 800 µm 1000 µm

Profilfunktion: Trockenkühler Vakuumier Material aus Engpassung: ja nein

Granulierung: GK Frequenz GK CEI Ecom ELG400 FR 3 - kurz FR 3 - lang FR 4 - kurz FR 4 - lang FR 5.5 - kurz FR 5.5 - lang FR 6 - UPM Sesselschiebe Plato 10005 Bineozeltopf Proprüf 104 Strengplatte

Bemerkung: *• In letzter 1/4 des Flusses
mit 100 erweichte Verwindung
einsetzte / nicht optimal
Verwindung des PLA
(erweichung) +5°C bei
Säulen T2 / T3*